Available online at www.sciencedirect.com

ScienceDirect

Procedia Engineering00 (2015) 000–000

Procedia Engineering

www.elsevier.com/locate/procedia

6th BSME International Conference on Thermal Engineering (ICTE 2014)

Unsteady MHD Casson Fluid Flow through a Parallel Plate with Hall Current

Md. Afikuzzaman, M. Ferdows and Md. Mahmud Alam*

Mathematics Discipline, Khulna University, Khulna-9208, Bangladesh
***Mathematics Department, Dhaka University, Dhaka-1000, Bangladesh*

Abstract

Unsteady MHD Casson fluid flow through a parallel plate with hall current is investigated. The uniform magnetic field is applied perpendicular to the plates and the fluid motion is subjected to a uniform suction and injection. The lower plate is stationary and the upper plate is moving. Explicit Finite Difference technique has been used to solve the momentum and energy equations. The effect of pressure gradient, the Hall parameter and other parameters describing in the equations are shown graphically. Effect of decaying parameter with different Casson number on primary velocity, secondary velocity and temperature distributions are illustrated in the form of the graph.

Peer-review under responsibility of organizing committee of the 6th BSMEInternational Conference on Thermal Engineering (ICTE 2014).

Keywords: MHD; Heat Transfer; Hall Current; Finite Difference Techniques.

1. Introduction

In recent years, there has been considerable interest in the magnetohydrodynamic effect of viscous incompressible non-Newtonian Casson fluid flow with heat transfer with or without hall currents. The flow of an electrically conducting viscous fluid through a parallel plate in the presence of a transversely applied magnetic field has applications in many devices such as magnetohydrodynamic (MHD) power generators, MHD pumps, accelerators, aerodynamics heating, electrostatic precipitation, polymer technology, petroleum industry, pharmaceutical process, purification of crude oil, fluid droplets sprays etc. The most important non-Newtonian fluid possessing a yield value is the Casson fluid, which are carried significant applications in polymer processing

* Corresponding author. Tel.:+88-041-725741; Cell: +8801912982811 fax:+88-041-731244
*E-mail address:*alam_mahmud2013@ku.ac.bd

Peer-review under responsibility of organizing committee of the 6th BSME International Conference on Thermal Engineering (ICTE 2014).

industries and biomechanics. Casson fluid is a shear thinning liquid which has an infinite viscosity at a zero rate of strain. Casson's constitute equation represents a nonlinear relationship between stress and rate of strain and has been found to be accurately applicable to silicon suspensions, suspensions of bentonic in water and lithographic varnishes used for printing inks. The fluid is acted upon by a constant pressure gradient and is subjected to a uniform magnetic field perpendicular to the plates. The Hall current is taken into consideration while the induced magnetic field is neglected by assuming a very small magnetic Reynolds number. The configuration is a good approximation of some practical situations such as heat exchangers, flow meters and pipes that connects system components. Walawander et al. [1] studied approximate Casson fluid model for tube flow of blood. Batra and Jena [2] showed the flow of a Casson fluid in a slightly curved tube. Attia [3] discussed unsteady MHD Couette flow and heat transfer of dusty fluid with variable physical property which is related to the Casson fluid. Attia and Sayed-Ahmed [4] analyzed Hydrodynamic impulsive Lid driven flow and heat transfer of a Casson fluid. Sayed-Ahmed et al. [5] examined time dependent pressure gradient effect on unsteady MHD couette flow and heat transfer of a casson fluid. Bhattacharyya et al. [6] showed analytic solution for magnetohydrodynamic boundary layer flow of Casson fluid.

Hence our main aim is to extend the work of Sayed-Ahmed et al. [5] and to investigate unsteady MHD Casson fluid flow through a parallel plate with hall current. The proposed model has been transformed into nonlinear coupled partial differential equations by usual transformation. Finally, the governing momentum and energy equations are solved numerically in case of one dimension flow and explicit finite difference method has been used to calculate the results and for stability analysis.

2. Mathematical formulation

Consider unsteady, viscous, viscous laminar and incompressible fluid flows between two infinite horizontal plates located at $y = \pm h$ planes and extended from $x = -\infty$ to ∞ and from $z = -\infty$ to ∞ .The upper plate moves with a uniform velocity U_0 while the lower plate is stationary. The upper and lower plates are kept at two constants temperature T_2 and T_1 respectively with $T_2 > T_1$. The fluid is acted upon by an exponentially decaying pressure gradient $\frac{\partial p}{\partial x}$ in the x direction and a uniform suction from above and injection from below which are applied at $t = 0$. A uniform magnetic field is applied in the positive y -direction and is assumed undistributed as the induced magnetic field is neglected by assuming a very small magnetic Reynolds number. The Hall Effect is taken into consideration and consequently a z -component for the velocity is expected to arise. The uniform suction implies that the *y*-component of the velocity v_0 is constant. Thus the fluid velocity vector is given by;

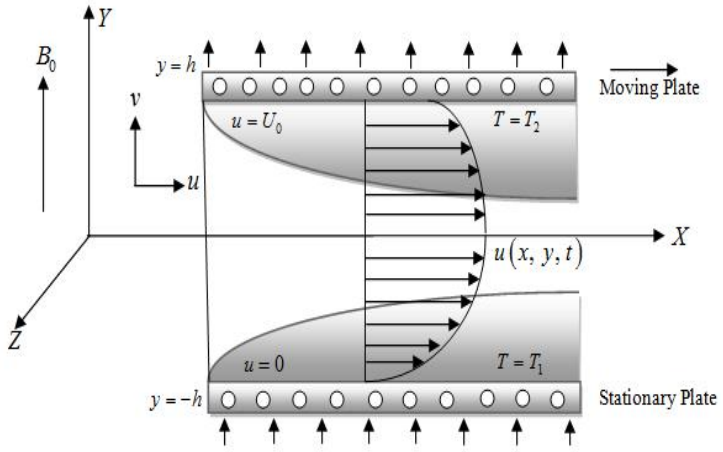

Figure 1: Geometrical configuration of thermal boundary layer.

$$v = u\mathbf{i} + v_0\mathbf{j} + w\mathbf{k}$$

The non-dimensional variables that have been used in the governing equations are

$$\bar{x} = \frac{x}{h},\ \bar{y} = \frac{y}{h},\ \bar{z} = \frac{z}{h},\ \bar{t} = \frac{tU_0}{h},\ \bar{u} = \frac{u}{U_0},\ \bar{w} = \frac{w}{U_0},\ \bar{p} = \frac{p}{\rho U^2{}_0},\ \theta = \frac{T - T_1}{T_2 - T_1},\ \bar{\mu} = \frac{\mu}{K_c{}^2}$$

Using these above dimensionless variables, the following dimensionless equations have been obtained as;

$$\frac{\partial u}{\partial t}+\frac{S}{\mathrm{Re}}\frac{\partial u}{\partial y}=-\alpha e^{-at}+\left[\frac{\partial}{\partial y}\left(\mu\frac{\partial u}{\partial y}\right)-\frac{{H_a}^2}{1+m^2}(u+mw)\right] \tag{1}$$

$$\frac{\partial w}{\partial t}+\frac{S}{\mathrm{Re}}\frac{\partial w}{\partial y}=\frac{1}{\mathrm{Re}}\left[\frac{\partial}{\partial y}\left(\mu\frac{\partial w}{\partial y}\right)-\frac{{H_a}^2}{1+m^2}(w-mu)\right] \tag{2}$$

$$\frac{\partial \theta}{\partial t}+\frac{S}{\mathrm{Re}}\frac{\partial \theta}{\partial y}=\frac{1}{P_r}\frac{\partial^2\theta}{\partial y^2}+E_c\mu\left[(\frac{\partial u}{\partial y})^2+(\frac{\partial w}{\partial y})^2\right]+\frac{{H_a}^2E_c}{(1+m^2)}(u^2+w^2) \tag{3}$$

$$\mu=\left[1+\left(\tau_D/\sqrt{(\frac{\partial u}{\partial y})^2+(\frac{\partial w}{\partial y})^2}\right)^{1/2}\right]^2 \tag{4}$$

where α is the constant pressure gradient $(\frac{dp}{dx})$ and a is the decaying parameter.

The corresponding non-dimensional boundary conditions are;

$t>0 \qquad u=0 \qquad w=0 \qquad T=0 \qquad at\ y=-1$

$\qquad\quad u=1 \qquad w=0 \qquad T=1 \qquad at\ y=1$

The non-dimensional quantities are; Casson number $\tau_D=\frac{\tau_0 h}{{k_c}^2U_0}$, Reynolds number $R_e=\frac{\rho U_0 h}{{k_c}^2}$, Suction parameter $S=\frac{\rho v_0 h}{{k_c}^2}$, Prandtl number $P_r=\frac{\rho c_p U_0 h}{k}$, Eckert number $E_c=\frac{U_0{k_c}^2}{\rho c_p h(T_2-T_!)}$, Hartmann number squared ${H_a}^2=\frac{\sigma{B_0}^2h^2}{{k_c}^2}$.

3. Numerical Solution

In this section the governing second order non-linear coupled dimensionless partial differential equations with initial and boundary conditions have been solved. The explicit finite difference method has been used to solve equations (1-4) subject to the boundary conditions. The region within the boundary layer is divided by some perpendicular line of Y-axis, where Y-axis is normal to the medium as shown in the figure. It is assumed that the maximum length of the boundary layer is $Y_{\max}=2$ i.e. Y varies from -1 to $+1$ and the number of grid spacing in Y direction is $m=100$. Hence the constant mesh size along Y-axis becomes $\Delta Y=0.02(-1\le Y\le 1)$ with smaller time step $\Delta t=0.0001$.

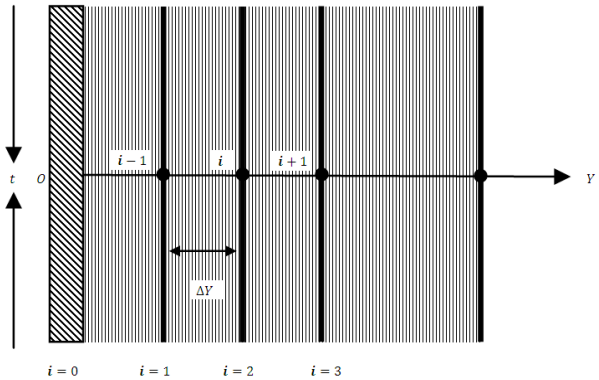

Figure 2: Finite difference space grid

Let $U',W'\ and\ \theta'$ denote the values $U,W\ and\ \theta$ at the end of a time step respectively. Using the explicit finite difference method the system of partial differential equation (1-3) is obtained an appropriate set of finite difference equations;

$$\frac{U_i^{n+1}-U_i^n}{\Delta t}+\frac{S}{R_e}\frac{U_{i+1}^n-U_i^n}{\Delta Y}=-\alpha e^{-at}$$
$$+\frac{1}{R_e}\left[\mu_i{}^n\frac{U_{i+1}^n-2U_i^n+U_{i-1}^n}{\Delta Y^2}+\frac{\mu_{i+1}^n-\mu_i^n}{\Delta Y}\frac{U_{i+1}^n-U_i^n}{\Delta Y}-\frac{H_a^2}{1+m^2}\left(U_i^n+mW_i^n\right)\right] \quad (5)$$

$$\frac{W_i^{n+1}-W_i^n}{\Delta t}+\frac{S}{R_e}\frac{W_{i+1}^n-W_i^n}{\Delta Y}=$$
$$+\frac{1}{R_e}\left[\mu_i{}^n\frac{W_{i+1}^n-2W_i^n+W_{i-1}^n}{\Delta Y^2}+\frac{\mu_{i+1}^n-\mu_i^n}{\Delta Y}\frac{W_{i+1}^n-W_i^n}{\Delta Y}-\frac{H_a^2}{1+m^2}\left(W_i^n-mU_i^n\right)\right] \quad (6)$$

$$\frac{\theta_i^{n+1}-\theta_i^n}{\Delta t}+\frac{S}{R_e}\frac{\theta_{i+1}^n-\theta_i^n}{\Delta Y}=$$

$$\frac{1}{P_r}\left[\frac{\theta_{i+1}^n-2\theta_i^n+\theta_{i-1}^n}{\Delta Y^2}\right]+E_c\mu\left[\left(\frac{U_{i+1}^n-U_i^n}{\Delta Y}\right)^2+\left(\frac{W_{i+1}^n-W_i^n}{\Delta Y}\right)^2\right]+\frac{H_a{}^2E_c}{(1+m^2)}\left[\left(U_i^n\right)^2+\left(W_i^n\right)^2\right] \quad (7)$$

and the initial and boundary conditions with the finite difference scheme are

$t>0$ $\quad U_L{}^n=0,\quad W_L{}^n=0,\quad \theta_L{}^n=0 \quad$ *where* $L=-1$

$\quad U_L{}^n=1,\quad W_L{}^n=0,\quad \theta_L{}^n=1 \quad$ *where* $L=1$

4. Results and Discussion:

To obtain the steady-state solutions, the computations have been carried out up to dimensionless time $t=0$ to 20. The results of the computations, however, show little changes in the above mentioned quantities after dimensionless time $t=5$. Thus the solutions for dimensionless time $t=5$ are essentially steady-state solutions. To observe the physical situation of the problem, the steady-state solutions have been illustrated in figures 3-7.

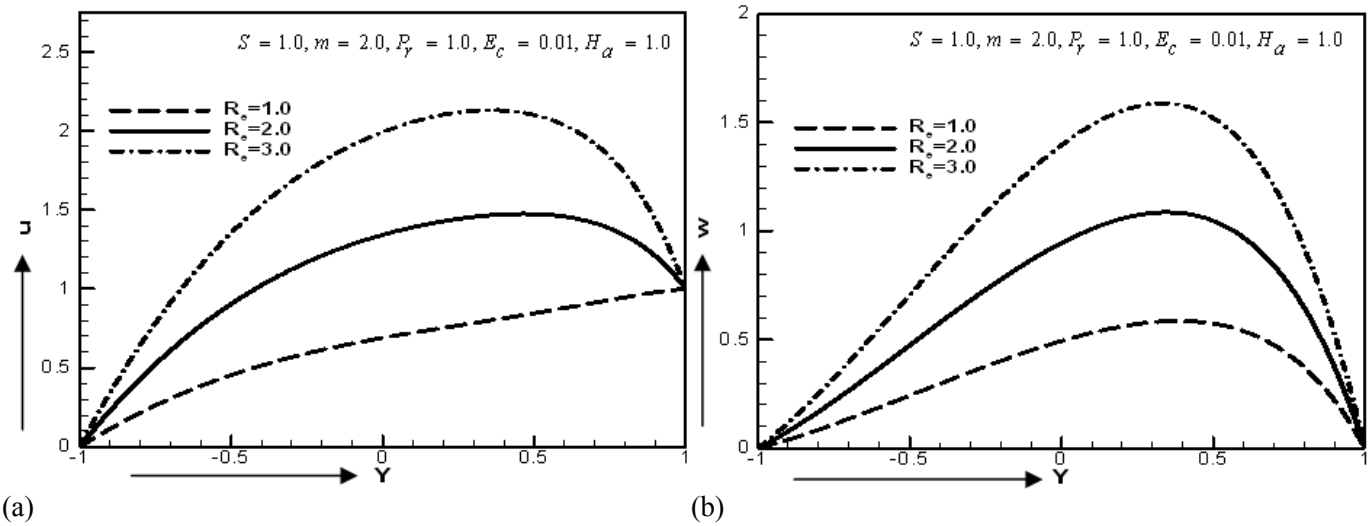

(a) (b)

Figure 3: (a) Primary velocity distribution and (b) secondary velocity distributions for different values of Reynolds number at *t=5.0*

The primary and secondary velocity distributions have been shown in figures 3(a) and 3(b) for different values of Reynolds number. Both the primary and secondary velocity distributions have been increased with the increase of R_e.

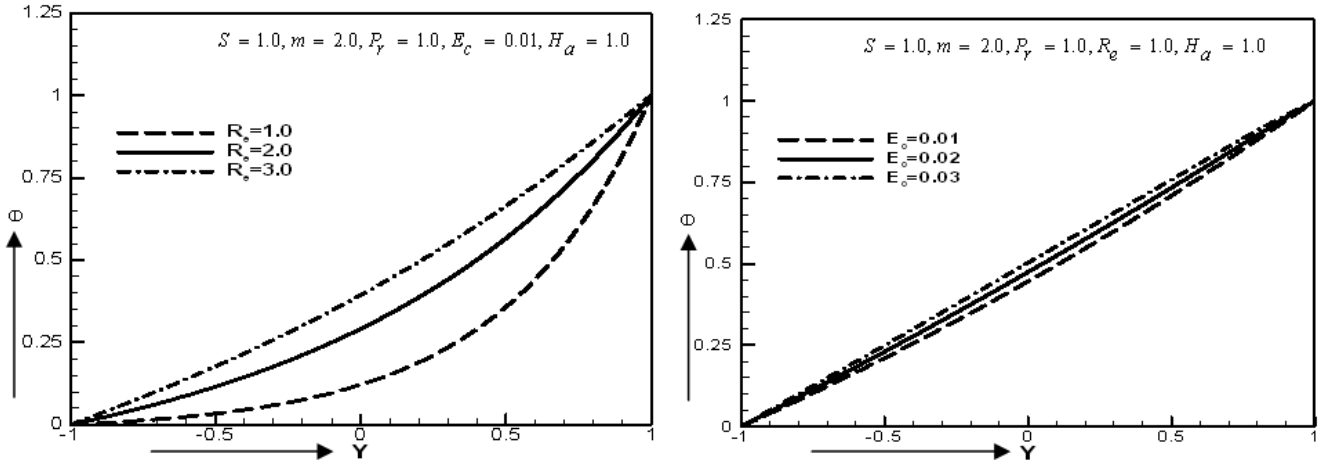

(a) (b)

Figure 4: (a) Temperature distribution for different values of Reynolds number and (b) Temperature distributions for different values of Eckert number at *t*=5.0

The temperature distributions have been shown in figure 4(a) and 4(b) for different values of Reynolds number R_e and Eckert number E_c respectively. In both cases the temperature distribution increases with the increase of R_e and E_c .It is shown from figure 5(a) and 5(b) the primary velocity component decreases with increasing decaying parameter for all values of τ_D. It is observed that the time at which primary velocity reaches its steady state value decreases with increasing a for $a > 0$. Increasing τ_D increases primary velocity for all values of decaying parameter but with small difference.

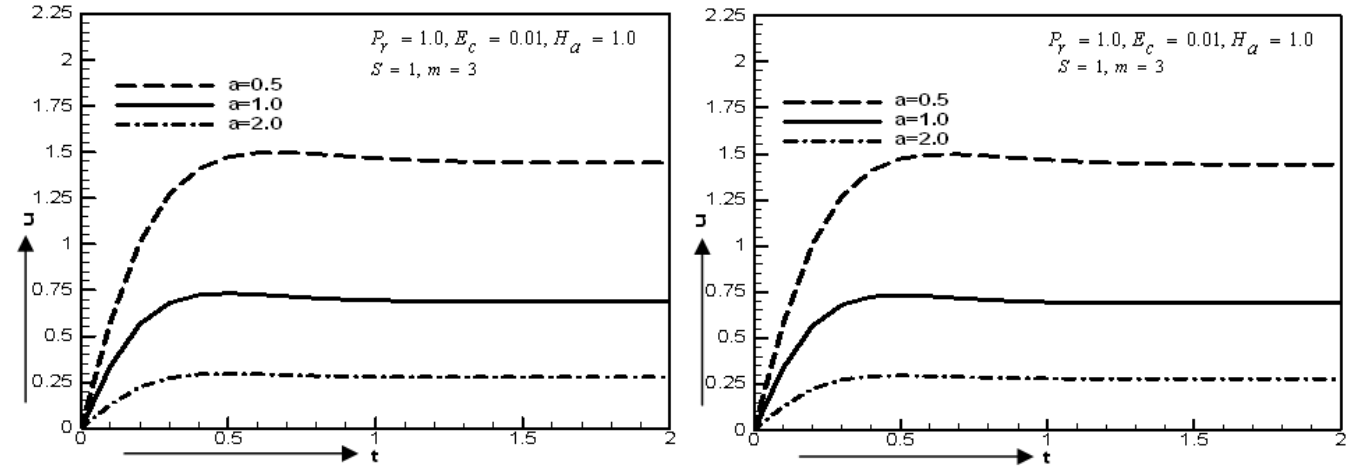

(a) (b)

Figure 5: (a) Effect of decaying parameter a on primary velocity at $y = 0$ for $\tau_D = 0.05$ and (b) Effect of decaying parameter a on primary velocity at $y = 0$ for $\tau_D = 0.1$

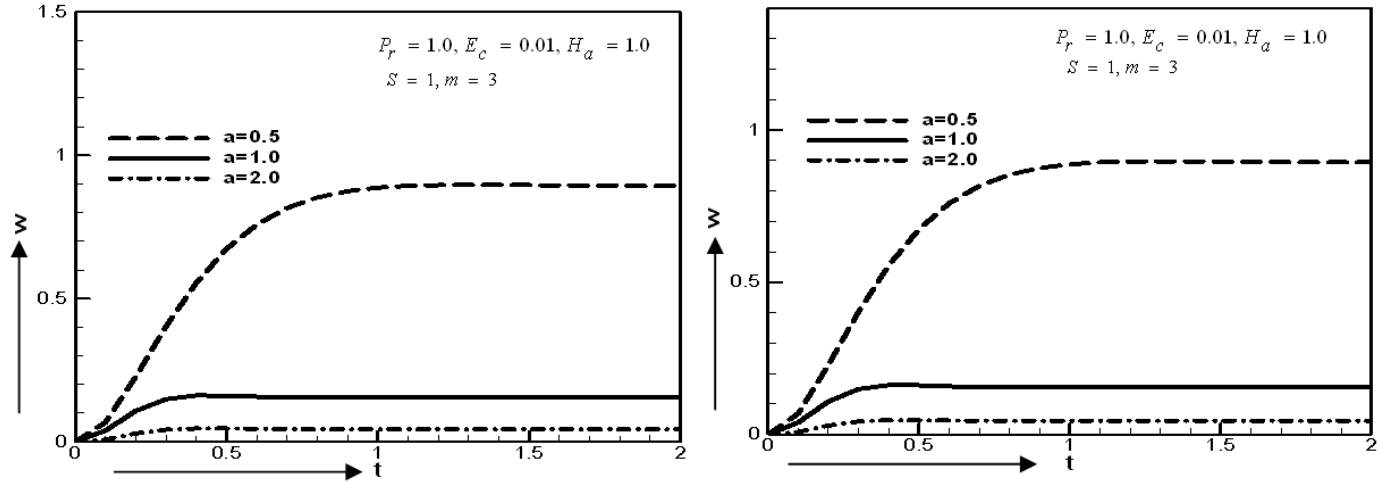

Figure 6: (a) Effect of decaying parameter a on secondary velocity at $y = 0$ for $\tau_D = 0.05$ and (b) Effect of decaying parameter a on secondary velocity at $y = 0$ for $\tau_D = 0.1$

The secondary velocity distributions have been shown in figure 6(a) and 6(b) for different values of τ_D with different decaying parameter. It is observed that secondary velocity component decreases with increasing decaying parameter. These figures indicate that the influence of τ_D on secondary velocity depends on t and become more clear when decaying parameter near to zero but this influence is small for large a. From the figure 7(a) and 7(b), it have been shown that influence of decaying parameter on temperature distributions depend on t. It is also shown that increasing a decreases θ while it is not greatly affected by changing τ_D.

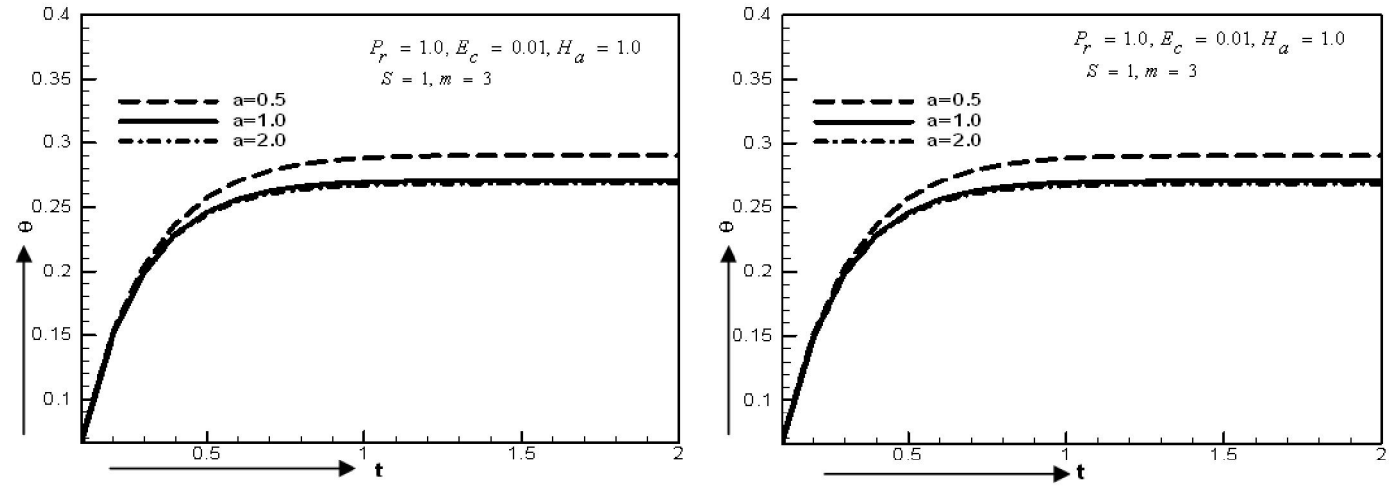

Figure 7: (a) Effect of decaying parameter a on temperature at $y = 0$ for $\tau_D = 0.05$ and (b) Effect of decaying parameter a on temperature at $y = 0$ for $\tau_D = 0.1$

Conclusions:

In this research work, the explicit finite difference method of unsteady one dimensional Casson non-Newtonian fluid flow through a parallel plate with a hall current is investigated. The physical properties are illustrated graphically for different values of parameter. The primary velocity, secondary velocity and temperature distributions have been increased with the increase of Reynolds number. The effect of decaying parameter a, Casson fluid yield stress τ_D, and the Hall parameter m, on the velocity and temperature distributions are studied. The decaying parameter a affects the main velocity components and the temperature. The result shows that the influence of the parameters a and τ_D on velocity components and the temperature depends on Hall parameter m and suction parameter S. The time at which two velocity component reach the steady state increases with increasing m, but decreases when τ_D increases. The time at which θ reaches its steady state increases with increasing m while it is not greatly affected by changing τ_D.

References:

[1] Walawander W.P., Chen T.Y. and Cala D.F., "An approximate Casson Fluid Model for tube flow of Blood", *Biorheology,* vol. 12, No. 2 19 75, pp. 111-124.

[2] Batra R.L. and Jena B. "Flow of a Casson Fluid in a slightly Curved tube", *International Journal of Engineering Science*, Vol. 29, No. 10, 1991, pp. 1245-1258.

[3] Attia H. A. ''Unsteady MHD Couetee Flow and Heat Transfer of Dusty Fluid with variable Physical properties,'' *Applied Mathematics and Computation*, Vol. 177, No. 1, 2005, pp. 308-318.

[4] Attia H.A. and M.E. Sayed-Ahmed, ''Hydrodynamic Impulsive Lid Driven Flow and Heat Transfer of a Casson Fluid'', *Tamakang Journal of Science and Engineering*, Vol. 9, No.3, 2006, pp. 195-204.

[5] M. E. Sayed-Ahmed, H. A. Attia, and K. M. Ewis, ''Time Dependent Pressure Gradient Effect on Unsteady MHD Couette Flow and Heat Transfer of a Casson Fluid'', Canadian Journal of Physics, Vol. 3, No.1 (2011), pp. 38-49.

[6] K. Bhattacharyya, T. Hayat and A. Alsaedi, ''Analytic solution for magnetohydrodynamic boundary layer flow of Casson fluid over a stretching/shrinking sheet with wall mass transfer", *Journal of Chinese Physics B*, Vol. 22, Article ID 024702, 2013.

Available online at www.sciencedirect.com

ScienceDirect

Procedia Engineering00 (2015) 000–000

Procedia Engineering

www.elsevier.com/locate/procedia

6th BSME International Conference on Thermal Engineering (ICTE 2014)

Unsteady MHD viscous incompressible Bingham fluid flow with hall current

Afroja Parvin*, Tanni Alam Dola** and Md. Mahmud Alam ***

*The Abdus Salam International Centre for Theoretical Physics, Strada Costiera 11, I-34151 Trieste, Italy

**Department Civil Engineering, Bangladesh University of Engineering and Technology(BUET), Dhaka-1000, Bangladesh

***Mathematics Discipline, Science, Engineering and Technology School, Khulna University, Khulna-9208, Bangladesh

Abstract

An electrically conducting viscous incompressible Bingham fluid bounded by two parallel non-conducting plates has been investigated in the presence of Hall current. The fluid motion is uniform at the upper plate and the uniform magnetic field is applied perpendicular to the plate. The lower plate is fixed while upper plate moves with a constant velocity. The governing equations have been non-dimensionalzed by using usual transformations. The obtained governing non-linear coupled partial differential equations have been solved by using explicit finite difference technique. The numerical solutions are obtained for momentum and energy equations. The influence of various interesting parameters on the flow has been analyzed and discussed through graph in details. The values of Local Nusselt number, Average Nusselt number, local Skin- Friction, Average Skin-Friction for different physical parameters are also illustrated in the form of graph.

Peer-review under responsibility of organizing committee of the 6th BSMEInternational Conference on Thermal Engineering (ICTE 2014).

Keywords: MHD Flow; Hall parameter; Explicit finite difference technique; Stability analysis

1. Introduction

The study about magnetohydrodynamic (MHD) flow has received considerable attention to many researchers due to its many industrial applications such as the use of MHD pumps in chemical industry technology for filtration and purification process, the operations of MHD accelerators, aerodynamics heating, electrostatics precipitation,

*** Corresponding author. Tel.:+88-041-725741; fax:+88-041-731244

***E-mail address:alam_mahmud2000@yahoo.com

Peer-review under responsibility of organizing committee of the 6th BSME International Conference on Thermal Engineering (ICTE 2014).

polymer technology, petroleum industry and fluid droplets sprays. The steady MHD flow between two infinite parallel stationary plates in the presence of a transverse uniform magnetic field was first studied Attia[1].

Nomenclature

u, w	Velocity components
T_1, T_2	Temperature at lower and upper plates
B_o	Uniform magnetic field
U, W	Primary and secondary velocity
θ	Dimensionless temperature
τ_D	Dimensionless Bingham number
τ	Dimensionless time
m	Hall parameter
H_a	Hartmann number
P_r	Prandtl number
E_c	Eckert number
R_E	Reynolds number

Such type of flow can be used in Civil engineering point of view. For bridge construction, the water flow between two piers can be measured and also the appropriate distance between the two piers can be measured.

Last few decades, great emphasis had been laid on continuum mechanics with paying particular attention on polymer solutions and polymer melts. But many geological and industry materials such as mud, lava, painting oil, drilling mud, cement, sludge, grease, granular suspensions, chocolate and paper pulp, which are frequently used in industrial problems which includes viscoplastic materials such as Bingham plastic named Bingham.

It is of special class, for which the shear stress beyond the yield stress is linearly proportional to the shear rate. If the yield stress tends to zero, the Bingham plastic fluid can entirely be treated as Newtonian fluid. But viscoplastic Couette flow, more precisely Bingham-Couette flow under the action of magnetic field applied perpendicularly has application in MHD power generators, MHD pumps, accelerators, electrostatic precipitation. In the study of the channel flow of the Bingham fluid, Friggard [2] mentioned that an infinitesimal perturbation to the flow should displace the yield surfaces but otherwise leave them intact, since the unyielded region is "an elastic solid that would not break up". Attia [3] studied the effects of Hall current on unsteady MHD couette flow and heat transfer on Bingham fluid with suction and injection. Naik *et al.* [4] studied the effect of Hall current on unsteady MHD free connective couette flow of Bingham fluid with thermal radiation. Crank Nicolson finite difference technique was used to obtain exact solution for velocity and temperature field with the effect of thermal radiation and Hall parameter.

In this paper, our aim is to study the finite difference solution of unsteady MHD viscous incompressible Bingham fluid flow with hall current. The system is considered as such that the upper plate is moving with a uniform velocity while the lower plate is fixed. A constant pressure gradient act on the plastic flow and uniform magnetic field is applied perpendicular to the plates. Very small value of Magnetic Reynolds Number is assumed to neglect the strong effect of induced magnetic field. The governing momentum and energy equations are solved numerically using the explicit finite difference approximations. Eventually interesting effects on velocity and temperature distributions, Skin friction and Nusselt number at both plates for Bingham fluid is observed. Such type of model can be used for fluid flow between two piers.

2. Mathematical formulation

The physical configuration and the boundary condition of the problem is shown in Fig: 1. The fluid is assumed to be laminar, incompressible and obeying Bingham model and flows between two infinite horizontal plates. These plates are located at the $y = \pm h$ planes and extend from $x = 0$ to ∞ and from $z = 0$ to ∞. The upper plate moves with a uniform velocity U_0 while the lower plate is stationary. Both the upper and lower plates are kept at two constant temperatures are T_2 and T_1 respectively, with $T_2 > T_1$. A constant pressure gradient applied in the x-direction, and a uniform magnetic field B_0 is applied in the positive y-direction and is assumed undisturbed as the induced magnetic field is neglected by assuming a very small magnetic Reynolds number. Due to consideration of Hall Effect a z component for the velocity is expected to arise. Thus the fluid velocity vector is $\mathbf{q} = u\hat{i} + v\hat{j} + w\hat{k}$

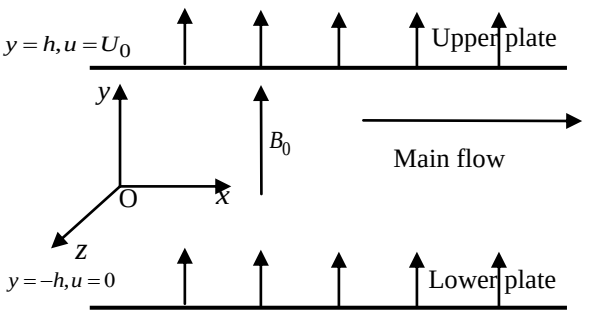

Fig: 1. The geometrical configuration

By using generalized Ohm's Law, the unsteady MHD Bingham fluid flows are governed by the following equations is given by;

Continuity equation: $$\frac{\partial u}{\partial x} + \frac{\partial v}{\partial y} = 0 \tag{1}$$

Momentum equation in x axis: $$\frac{\partial u}{\partial t} + u\frac{\partial u}{\partial x} + v\frac{\partial u}{\partial y} = -\frac{1}{\rho}\frac{dp}{dx} + \frac{1}{\rho}\frac{\partial}{\partial y}\left(\mu\frac{\partial u}{\partial y}\right) - \frac{1}{\rho}\left[\frac{\sigma {B_o}^2}{1+m^2}(u + mw)\right] \tag{2}$$

Momentum equation in z axis: $$\frac{\partial w}{\partial t} + u\frac{\partial w}{\partial x} + v\frac{\partial w}{\partial y} = \frac{1}{\rho}\frac{\partial}{\partial y}\left(\mu\frac{\partial w}{\partial y}\right) - \frac{1}{\rho}\left[\frac{\sigma {B_o}^2}{1+m^2}(w - mu)\right] \tag{3}$$

Energy equation: $$\frac{\partial T}{\partial t} + u\frac{\partial T}{\partial x} + v\frac{\partial T}{\partial y} = \frac{k}{\rho c_p}\frac{\partial^2 T}{\partial y^2} + \frac{\mu}{\rho c_p}\left[\left(\frac{\partial u}{\partial y}\right)^2 + \left(\frac{\partial w}{\partial y}\right)^2\right] + \frac{1}{\rho c_p}\left[\frac{\sigma {B_o}^2}{1+m^2}\left(u^2 + w^2\right)\right] \tag{4}$$

$\mu = \mathrm{K} + \dfrac{\tau_o}{\sqrt{\left(\frac{\partial u}{\partial y}\right)^2 + \left(\frac{\partial w}{\partial y}\right)^2}}$ is the apparent viscosity of Bingham fluid

with the corresponding boundary conditions are

$$\begin{array}{ll} & u = 0,\ w = 0, \mathrm{T} = \mathrm{T}_1 \quad \text{at x} = 0 \\ t > 0 & u = 0,\ w = 0, \mathrm{T} = \mathrm{T}_1 \quad \text{at } y = -h \\ & u = U_o, w = 0, \mathrm{T} = \mathrm{T}_2 \ \text{at } y = h \end{array}$$

To obtain the governing equations and the boundary condition in dimensionless form the following non-dimensional quantities are used as;

$$X = \frac{x}{h}, Y = \frac{y}{h}, Z = \frac{z}{h}, U = \frac{u}{U_o}, V = \frac{v}{U_o}, W = \frac{w}{U_o}, P = \frac{p}{\rho {U_o}^2}, \tau = \frac{tU_o}{h}, \theta = \frac{T - T_1}{T_2 - T_1}, \bar{\mu} = \frac{\mu}{k}$$

Using the above non-dimensional variables in equations (1- 4) and boundary conditions it can be written as (where hat is dropped)

$$\frac{\partial U}{\partial X}+\frac{\partial V}{\partial Y}=0 \tag{5}$$

$$\frac{\partial U}{\partial \tau}+U\frac{\partial U}{\partial X}+V\frac{\partial U}{\partial Y}=-\frac{dP}{dX}+\frac{1}{R_{\mathrm{E}}}\left[\frac{\partial}{\partial Y}\left(\mu\frac{\partial U}{\partial Y}\right)-\frac{{H_a}^2}{\left(1+m^2\right)}\left(U+mW\right)\right] \tag{6}$$

$$\frac{\partial W}{\partial \tau}+U\frac{\partial W}{\partial X}+V\frac{\partial W}{\partial Y}=\frac{1}{R_{\mathrm{E}}}\left[\frac{\partial}{\partial Y}\left(\mu\frac{\partial W}{\partial Y}\right)-\frac{{H_a}^2}{\left(1+m^2\right)}\left(W-mU\right)\right] \tag{7}$$

$$\frac{\partial \theta}{\partial \tau}+U\frac{\partial \theta}{\partial X}+V\frac{\partial \theta}{\partial Y}=\frac{1}{P_r}\frac{\partial^2\theta}{\partial Y^2}+\mathrm{E}_c\mu\left[\left(\frac{\partial U}{\partial Y}\right)^2+\left(\frac{\partial W}{\partial Y}\right)^2\right]+\frac{{H_a}^2E_c}{\left(1+m^2\right)}\left(U^2+W^2\right) \tag{8}$$

$$\mu=1+\frac{\tau_D}{\sqrt{\left(\frac{\partial U}{\partial Y}\right)^2+\left(\frac{\partial W}{\partial Y}\right)^2}}$$

And the dimensionless boundary conditions are;

$$\begin{array}{ll} & U=0,\ \mathrm{W}=0,\theta=0 \quad \text{at X} = 0 \\ \tau>0 & U=0,\ \mathrm{W}=0,\theta=0 \quad \text{at Y} = -1 \\ & U=1,\ \mathrm{W}=0,\theta=1 \quad \text{at Y} = 1 \end{array}$$

3. Shear Stress and Nusselt Number

From the velocity field, the effects of various parameters on Shear Stress have been studied. Shear Stress in x direction for stationary wall is $\tau_{w1}=\left[\mu\sqrt{\left(\frac{\partial U}{\partial Y}\right)^2+\left(\frac{\partial W}{\partial Y}\right)^2}\right]_{Y=-1}$ and for moving wall is $\tau_{w2}=\left[\mu\sqrt{\left(\frac{\partial U}{\partial Y}\right)^2+\left(\frac{\partial W}{\partial Y}\right)^2}\right]_{Y=1}$

From the temperature field, the effects of various parameters on Nusselt number have been analyzed. Nusselt Number for stationary wall is $N_{u1}=\frac{\left(2\frac{\partial T}{\partial Y}\right)_{Y=-1}}{-T_m}$ and for moving wall is $N_{u2}=\frac{\left(2\frac{\partial T}{\partial Y}\right)_{Y=1}}{-\left(T_m-1\right)}$, where T_m is the dimensionless mean fluid temperature and is given by $T_m=\left(2\int_{-1}^{1}U\theta dY\Big/\int_{-1}^{1}UdY\right)$.

4. Numerical Solutions

To solve the non-dimensional system by explicit finite difference method, a set of finite difference equations is required. For this reason the area within the boundary layer is divided into a grid or mesh of lines parallel to x and y axis. Where x axis is taken along the plate and y axis is normal to the plate as shown in Fig: 2. It is considered that the plate of height $X_{\max}(=40)$ i.e. X varies from 1 to 40 and regard $Y_{\max}(=2)$ i.e. Y

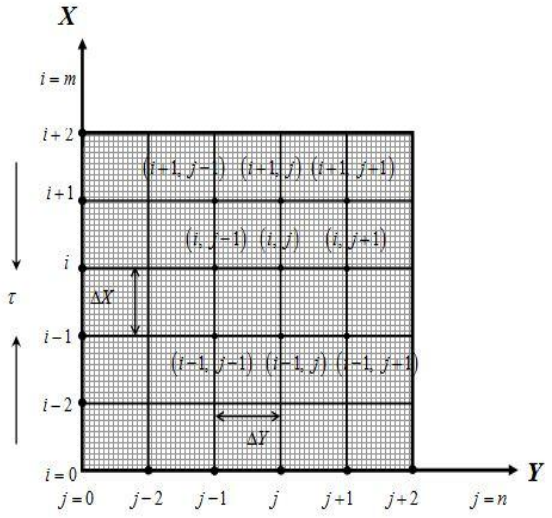

Fig: 2. Finite difference system grid

varies from 1 to 2. The number of grid spacing in both directions are $m=40, n=40$. Hence the constant mesh size along x and y directions are $\Delta x=1.0$ and $\Delta y=0.05$ respectively with smaller time step $\Delta\tau=0.0001$.

Let U', W' and θ' denotes the value of U, W and θ and the end of the time-step respectively. Using explicit finite difference, the following appropriate set of finite difference equation are obtained as;

$$\frac{U_{i,j}-U_{i-1,j}}{\Delta x}+\frac{V_{i,j}-V_{i-1,j}}{\Delta y}=0 \tag{9}$$

$$\frac{U_{i,j}'-U_{i,j}}{\Delta\tau}+U_{i,j}\frac{U_{i,j}-U_{i-1,j}}{\Delta X}+V_{i,j}\frac{U_{i,j+1}-U_{i,j}}{\Delta Y}= -\frac{dP}{dX}+\frac{1}{R_{\mathrm{E}}}\left[\left(\frac{\mu_{i,j+1}-\mu_{i,j}}{\Delta Y}\right)\left(\frac{U_{i,j+1}-U_{i,j}}{\Delta Y}\right)+\mu_{i,j}\left(\frac{U_{i,j+1}-2U_{i,j}+U_{i,j-1}}{\Delta Y^2}\right)-\frac{H_a{}^2}{1+m^2}\left(U_{i,j}+mW_{i,j}\right)\right] \tag{10}$$

$$\frac{W_{i,j}'-W_{i,j}}{\Delta\tau}+U_{i,j}\frac{W_{i,j}-W_{i-1,j}}{\Delta X}+V_{i,j}\frac{W_{i,j+1}-W_{i,j}}{\Delta Y}= \frac{1}{R_{\mathrm{E}}}\left[\left(\frac{\mu_{i,j+1}-\mu_{i,j}}{\Delta Y}\right)\left(\frac{W_{i,j+1}-W_{i,j}}{\Delta Y}\right)+\mu_{i,j}\left(\frac{W_{i,j+1}-2W_{i,j}+W_{i,j-1}}{\Delta Y^2}\right)-\frac{H_a{}^2}{1+m^2}\left(W_{i,j}-mU_{i,j}\right)\right] \tag{11}$$

$$\frac{\theta_{i,j}'-\theta_{i,j}}{\Delta\tau}+U_{i,j}\frac{\theta_{i,j}-\theta_{i-1,j}}{\Delta X}+V_{i,j}\frac{\theta_{i,j+1}-\theta_{i,j}}{\Delta Y}=\frac{1}{P_r}\left[\frac{\theta_{i,j+1}-2\theta_{i,j}+\theta_{i,j-1}}{\Delta Y^2}\right] + E_c\left(\mu_{i,j}\right)\left[\left(\frac{U_{i,j+1}-U_{i,j}}{\Delta Y}\right)^2+\left(\frac{W_{i,j+1}-W_{i,j}}{\Delta Y}\right)^2\right]+\frac{H_a{}^2E_c}{1+m^2}\left[\left(U_{i,j}\right)^2+\left(W_{i,j}\right)^2\right] \tag{12}$$

With the finite difference boundary conditions

$$U_{i,L}=0, W_{i,L}=0, \theta_{i,L}=0 \text{ at } L=-1$$
$$U_{i,L}=1, W_{i,L}=0, \theta_{i,L}=1 \text{ at } L=1$$

The numerical values of local shear stress, local Nusselt number are evaluated by **Five point** approximate formula and the average shear stress, average Nusselt number are calculated by **Simpson's** $\frac{1}{3}$ integration rule. The stability conditions of the method are; $\frac{U\Delta\tau}{\Delta X}+\frac{|V|\Delta\tau}{\Delta Y}+\frac{\Delta\tau}{2R_{\mathrm{E}}}\frac{H_a{}^2}{\left(1+m^2\right)}\le 1$, $\frac{U\Delta\tau}{\Delta X}+\frac{|V|\Delta\tau}{\Delta Y}+\frac{2\Delta\tau}{P_r\left(\Delta Y\right)^2}\le 1$ and the convergence criteria of the problem are $H_a\le 10, R_{\mathrm{E}}\ge 0.00251, m\ge 1, P_r\ge 0.08$ with $E_c=0.1$.(details are not shown for brevity)

5. Results and Discussion

The obtained governing equations are non-linear, coupled partial differential equations which cannot be solved analytically. That's why, explicit finite difference technique has been used to solve these equations. To obtain the numerical solutions, the computations have been carried out up to $\tau=0.1$ to $\tau=20.00$. The results of computation show little changes for $\tau=0.1$ to $\tau=4.50$, but after that until $\tau=20.00$ the results remain approximately same. In order to get the clear concept of physical properties of the problem, the effects of two parameters namely Hall

parameter (m), Hartmann number (H_a) in the presence of Reynolds number (R_E), Prandtl number (P_r) and Eckert number (E_c) are represented graphically through Figs: (3- 6). The effects of Hall current (m) on Shear Stress both at stationary and moving plate are presented in Fig.3(a-b). It is observed that Shear Stress at both plates increase with the increase of m .This is due to the fact an increase in m decreases effective conductivity $(=\sigma/(1+m^2))$, hence magnetic dumping force on U . The effects of Hall parameter (m) on Nusselt number both at stationary and moving plate are elucidated in Fig. 4(a-b). As U and W increases with the increase of m, joule and viscous dissipations also increases for which temperature increases. But the reverse effects is observed for Nusselt number. The effects of Hartmann number (H_a) on shear stress for both plates are shown in Fig: 5(a-b). It is seen that with the increase of Hartmann number (H_a) shear stress decreases, showing the effect of dragging the magnetic field as Hartmann number gives a measure of the relative importance of drag forces resulting from magnetic induction and viscous forces. The effects of Hartmann number on Nusselt number are shown in Fig: 6(a-c). It is observed that with increase of (H_a) Nusselt number at both plates increases. Due to the incitement of convection by the magnetic field which results in a gradual increase of Nusselt number.

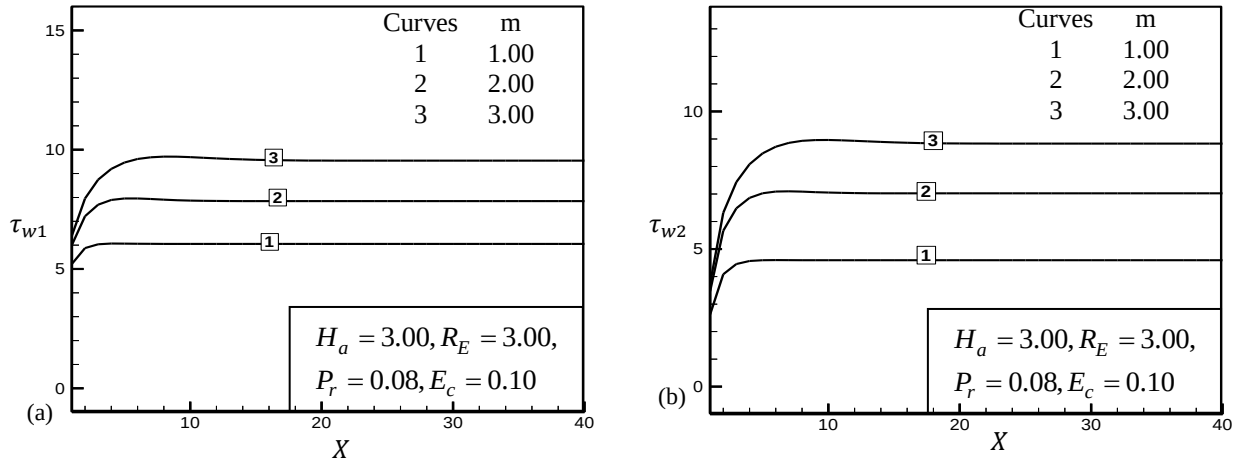

Fig: 3 Illustration of Shear Stress at (a) Stationary wall (b) Moving wall for different values of m

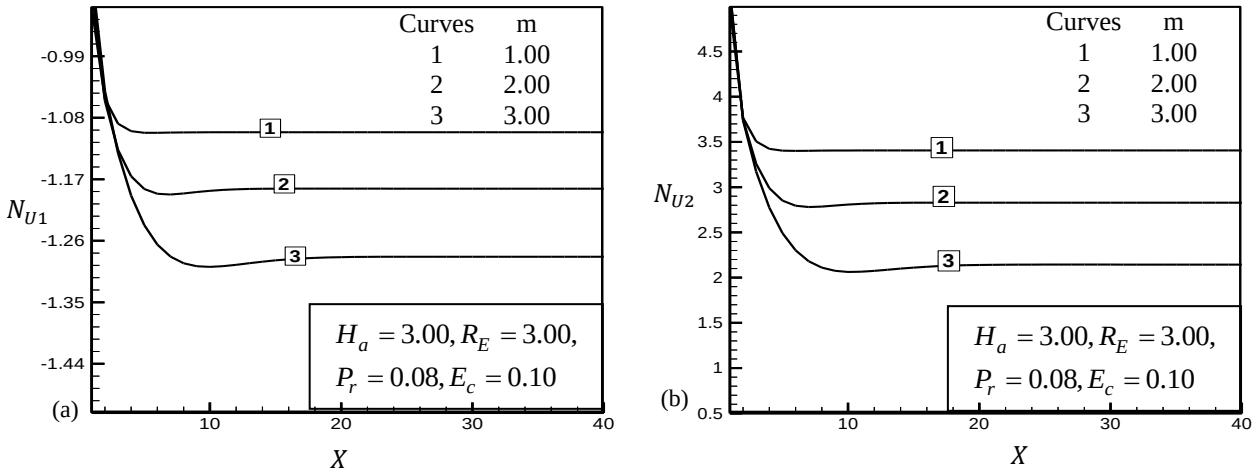

Fig: 4 Illustration of Nusselt Number at (a) Stationary wall (b) Moving wall for different values of m

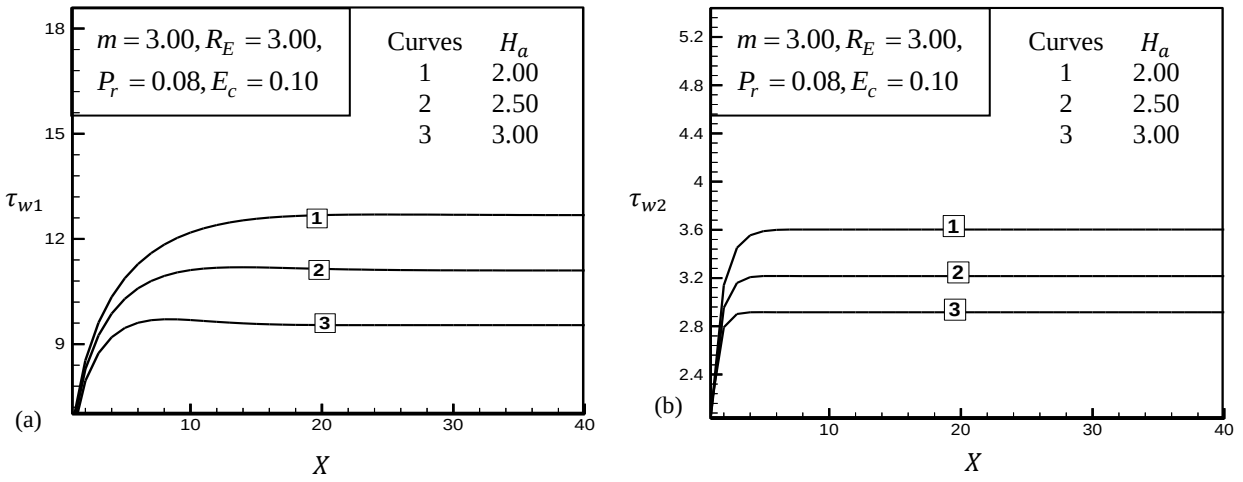

Fig: 5 Illustration of Shear Stress at (a) Stationary wall (b) Moving wall for different values of H_a

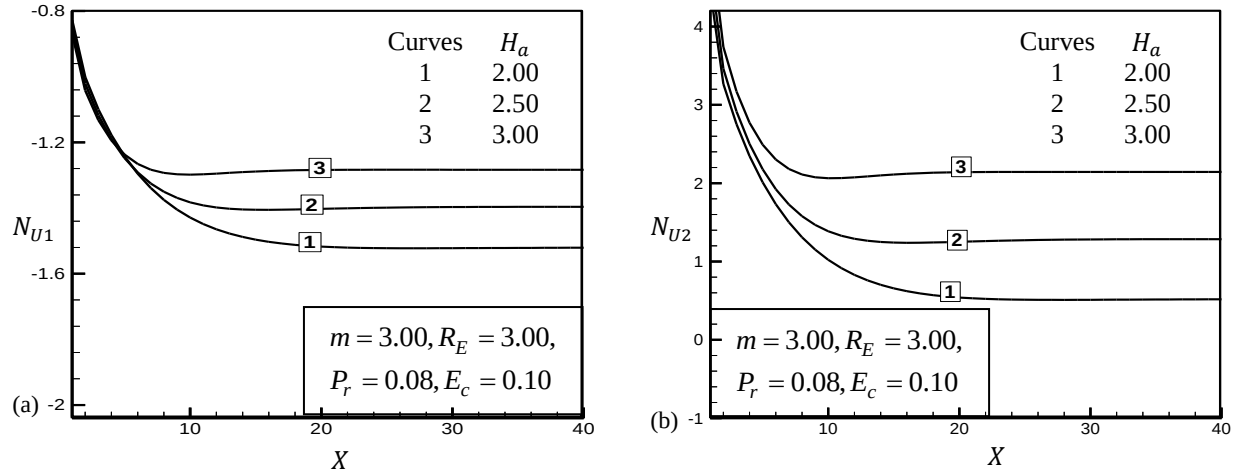

Fig: 6 Illustration of Nusselt Number at (a) Stationary wall (b) Moving wall for different values of H_a

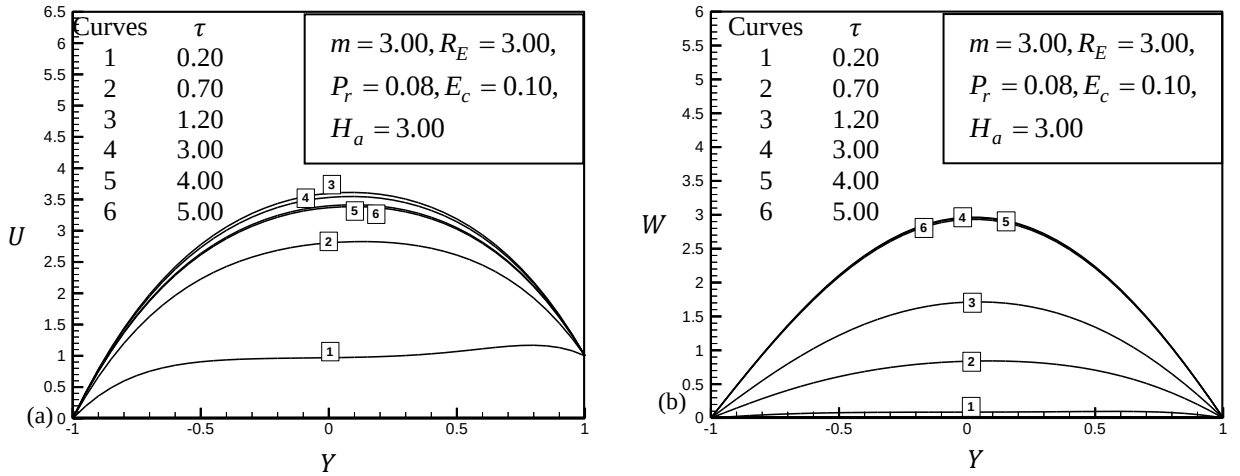

Fig: 7 Illustration of Time Variation for (a) Primary Velocity (b) Secondary Velocity

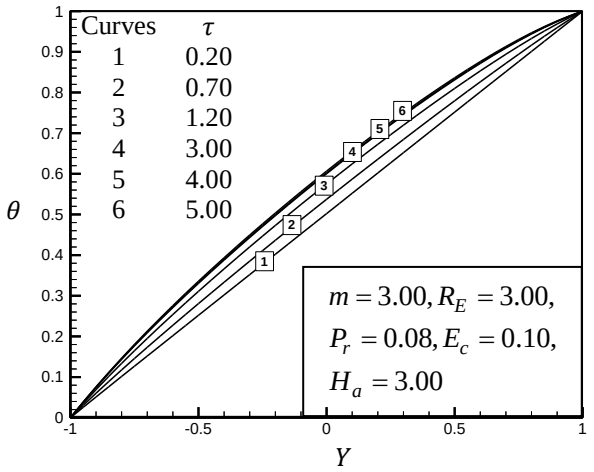

Fig: 8 Illustration of Time Variation for temperature

The profile of primary velocity, secondary velocity and temperature for different values of time step is shown in Fig: 7-8. It is seen from Fig: 7(a) that primary velocity does not reach its steady state monotonically. It increases with time up till a maximum value and then decrease up to steady state. But from Fig: 7(b) and Fig: 8 it is clear that both secondary velocity and temperature profiles reach their steady state monotonically. It also should be mentioned that primary velocity reaches the steady state faster than secondary velocity which, in turn, reaches steady state faster than temperature.

6. Conclusion

In this research, the explicit finite difference solution of unsteady MHD viscous incompressible Bingham fluid flow bounded by two electrically non-conducting plate in the presence of Hall current, Hartmann number, Reynolds number, Eckert number and Prandtl number has been investigated. For brevity, the effect of Eckert number and Prandtl number are not shown. The physical properties are illustrated graphically for different values of corresponding parameters. Among them some important findings of this investigation are mentioned here;

1. The Shear stress at stationary wall and moving wall increases with the increase of m.
2. The Nusselt number at stationary wall and moving wall decreases with the increase of m.
3. The Shear stress at stationary wall and moving wall decreases with the increase of H_a.
4. The Nusselt number at stationary wall and moving wall increases with the increase of H_a.
5. Primary velocity reaches steady state briskly in the comparison with secondary velocity and temperature.

References

1. H.A, Attia,., "On the Effectiveness of Variation in the Physical Variables on the Generalized Couette Flow with Heat Transfer in a Porous Medium", Research Journal of Physics, **1(1)**: 1-9, 2007.
2. I.A. Frigaard, S.D. Howison, I.J. Sobey (1994), One the stability of Poiseuille flow of a Bingham fluid, Journal of Fluid Mechanics 150(1994) pp.263:133
3. Hazem Ali Attia, Mohamed EissaSayed-Ahmedm, Hall effect on unsteady MHD Couette flow and heat of a Bingham fluid with suction and injection., Applied Mathematical Modelling 28(2004) pp. 1027–1045.
4. S. Harisingh Naik, K. Rama Rao, M. V. Ramana Murthy, The Effect of Hall Current on Unsteady MHDFree Convective Couette Flow of a Bingham Fluid with Thermal Radiation, International Journal of Engineering and Advanced Technology (IJEAT) ISSN: 2249 – 8958, Volume-3 Issue-6, August 2014.

Available online at www.sciencedirect.com

ScienceDirect

Procedia Engineering 00 (2015) 000–000

Procedia Engineering

www.elsevier.com/locate/procedia

6th BSME International Conference on Thermal Engineering (ICTE 2014)

Velocity and temperature distributions of laminar and transition boundary layer flows along a heated vertical flat plate

Mohammad Zoynal Abedin[a,*], Mohammed Moinul Islam[a], Mashud Rana[a], Jinho Lee[b]

[a]*Department of Mechanical Engineering, Dhaka University of Engineering & Technology, Gazipur-1700, Bangladesh*
[b]*School of Mechanical Engineering, Yonsei University, Seoul 120-749, Republic of Korea*

Abstract

Time-developing direct numerical simulation (DNS) has been performed for the laminar and transition boundary layer flows in the natural-convection and mixed-convection with aiding and opposing flows both in air and water along a heated vertical flat plate. The results reveal that the velocity profile of water in the laminar natural-convection boundary layer shows lower peak value compared to that in air and the temperature profile in water within the boundary layer becomes ambient at a shorter distance perpendicular to the heated wall compared to that in air due to the effects of higher Prandtl number of water. For laminar mixed-convection boundary layer, the velocity profile of water exhibits lower values throughout the boundary layer compared to that in air. In the case of opposing flows both in air and water, the velocity profiles show a sharp drop to a constant negative value in the outer boundary layer region. Furthermore, for transitional natural-convection boundary layer in air, the magnitude of the velocity profile increases with an increase in Grashof number due to the increasing trend in the boundary layer thickness. It is also found that the predicted heat transfer rates in the natural-convection boundary layer both in air and water correspond quantitatively well with the existing observations.

Peer-review under responsibility of organizing committee of the 6th BSME International Conference on Thermal Engineering (ICTE 2014).

Keywords: Laminar flow; Transitional flow; Boundary layer, Freestream velocity, Prandtl number, Natural convection, Mixed convection.

1. Introduction

The characteristics of the natural-convection and mixed-convection boundary layer flows are of great importance both from scientific and engineering viewpoints. The analysis of the boundary layer flows is important not only to

* Corresponding author. Tel.: +88-02-9204710; fax: +88-02-9204710.
E-mail address: abedin.mzoynal@duet.ac.bd (Mohammad Z. Abedin)

Peer-review under responsibility of organizing committee of the 6th BSME International Conference on Thermal Engineering (ICTE 2014).

clarify the fundamental characteristics of the boundary layer but also to evaluate the basic structures of the buoyancy-driven flows practically encountered in many applications. In most cases, freestream velocities are often superimposed on pure thermally-driven boundary layers (mixed-convection boundary layers) and the turbulence characteristics of the boundary layers vary with the magnitude and direction of freestream velocity and working fluids [1-3]. However, there are very limited investigations dealing with the time-developing DNS for the turbulent natural- and mixed-convection boundary layers along with their characteristics of the turbulent structures [4-7].

The fundamental characteristics of the turbulent natural-convection boundary layer along a heated vertical flat plate were extensively investigated by many researchers [8-18]. In some of these researches, advanced measurements and flow visualization have been done by using various experimental techniques in order to clarify the various characteristics. In addition, there are several numerical approaches performed for the turbulent natural-convection boundary layer to evaluate the characteristics of the boundary layer flows [19-21]. On the other hand, the fundamental characteristics of turbulent mixed-convection boundary layers were investigated along various passages [22-24] and the effects of freestream velocity on the turbulent mixed-convection boundary layer along a vertical heated plate were extensively investigated by Hattroi et al. [25-27]. Furthermore, few expensive experiments were conducted for the turbulent mixed-convection boundary layer with opposing flow (freestream in the direction to the gravitational force) [28, 29]. Due to the difficulty in obtaining the fluctuating characteristics of the boundary layer flows from the experiments, the numerical simulation techniques have been used to evaluate the characteristics of the complex flow phenomenon. Recently, the effects of freestream velocity on the characteristics of boundary layer flows have been numerically analyzed [3, 6]. However, the effects of both freestream velocity and Prandtl number on the characteristics of the boundary layer flows in the natural- and mixed-convection have not yet been focused sufficiently and are eagerly awaited.

Therefore, in the present analysis, the DNS has been employed to investigate the nature of the velocity and temperature distributions of the boundary layer flows under the influence of the freestream velocity and Prandtl number.

Nomenclature

c_p	specific heat at constant pressure, kJ/(kg K)
g	gravitational acceleration, m/s^2
Gr_x	Grashof number based on x from leading edge of plate in space-developing flow, $g\beta\Delta T_w x^3/\nu^2$
Gr_δ	Grashof number based on integral thickness δ, $g\beta\Delta T_w \delta^3/\nu^2$
k	thermal conductivity, W/(m K)
Nu_δ	Nusselt number based on integral thickness δ, hδ /k
p	pressure, Pa
Pr	Prandtl number, μ c_p /k
Re_δ	Reynolds number based on integral thickness δ, $U_\infty \delta/\nu$
T	mean temperature, K
t	instantaneous temperature, K
U	mean streamwise velocity, m/s
u	instantaneous streamwise velocity, m/s
U_0	characteristics velocity, ν/δ_0, m/s
v	instantaneous transverse velocity, m/s
w	instantaneous spanwise velocity, m/s
x	distance from leading edge of flat plate, m
x_i	coordinate in tensor notation, m
y	distance from heated wall, m
z	spanwise distance, m

Greek symbols

α	thermal diffusivity, m^2/s
β	coefficient of volume expansion, 1/K
θ	dimensionless temperature, $(t - T_\infty) / \Delta T_w$
ΔT_w	temperature difference between wall and ambient, $T_w - T_\infty$, K
δ	integral thickness of the velocity boundary layer, m
μ	viscosity, Pa.s
ν	kinematic viscosity, m^2/s
ρ	density, kg/m^3
τ	time, s

Superscripts

$*$	normalized variables with δ_0 andν for time-developing profiles

Subscripts

∞	ambient condition
0	initial condition
w	wall condition

2. Numerical procedure

A numerical investigation has been carried out for the natural- and mixed-convection boundary layer flows both in air and water along a heated vertical flat plate by time-developing DNS. The flow is induced by heating an infinitely long vertical flat plate at a uniform temperature from a given time onward ($\tau = 0$). The calculation domain and coordinate systems are shown in Fig. 1. The coordinates in the vertical, wall-normal and spanwise directions are x, y and z, respectively, and the instantaneous velocities u, v and w are specified in the relevant directions. The instantaneous temperature is t and the wall and ambient temperatures, T_w and T_∞, respectively, are assumed to be constant.

The governing equations with the Boussinesq approximation expressing the conservation of mass, momentum and energy in the tensor notation can be written as follows:

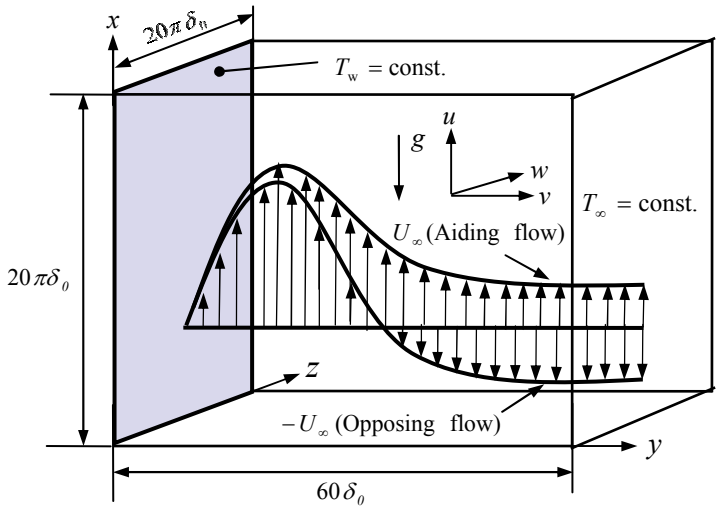

Fig. 1. Calculation domain and coordinates.

$$\frac{\partial u_i^*}{\partial x_i^*} = 0 \tag{1}$$

$$\frac{\partial u_i^*}{\partial \tau^*} + u_j^* \frac{\partial u_i^*}{\partial x_j^*} = -\frac{\partial p^*}{\partial x_i^*} + \frac{\partial^2 u_i^*}{\partial x_j^{*2}} + Gr_{\delta_0}\theta \tag{2}$$

$$\frac{\partial \theta}{\partial \tau^*} + u_j^* \frac{\partial \theta}{\partial x_j^*} = \frac{1}{Pr}\frac{\partial^2 \theta}{\partial x_j^{*2}} \tag{3}$$

Here, $Gr_{\delta_0} = g\beta\Delta T_w \delta_0^3/\nu^2$ is the Grashof number based on the integral thickness of the velocity boundary layer δ_0 and the superscript '*' denotes variables that have been made dimensionless with δ_0 and ν.

The periodic boundary conditions have been applied for the x^* and z^* directions and the boundary conditions in the y^* direction are provided as follows:

$$\begin{aligned} &y^* = 0: \; u^* = v^* = w^* = 0 \;,\; \theta = 1 \\ &y^* = 60: \; u^* = v^* = w^* = \theta = 0 \quad \text{for natural convection} \\ &y^* = 60: \; u^* = \frac{\pm U_\infty \delta_0}{\nu} = Re_{\delta_0},\; v^* = w^* = \theta = 0 \quad \text{for mixed convection} \end{aligned} \tag{4}$$

Here, $\frac{U_0\delta_0}{\nu} = 1$ and the sign $\pm$ of U_∞ corresponds to aiding and opposing flows, respectively. The above momentum and energy equations have been discretized by the second-order accurate central difference scheme on the staggered grids and the detailed numerical simulation techniques are extensively reported in the literature of Abedin et al. [1, 2].

The integral thickness of the velocity boundary layer δ, which is adopted as a characteristic length scale for the analysis, can be defined as:

$$\delta = \int_0^\infty \left|U - U_\infty\right| / \left(U_{max} - U_{min}\right) \, dy \tag{5}$$

Here, U is the mean velocity found by averaging the velocity in the (x - z) plane and U_{max} and U_{min} are the maximum and minimum mean velocities in the boundary layer, respectively. For pure natural convection, $U_{min} = U_\infty = 0$ and for mixed convection, $U_{min} = 0$ (aiding flow) and $U_{min} = -U_\infty$ (opposing flow).

3. Results and discussions

Time-developing DNS was advanced by adding various initial disturbances in the laminar boundary layer, which were created by reducing velocity fluctuations observed in the turbulent boundary layer to tiny fluctuations less than 5% for the intensities. Such disturbances added in the laminar boundary layer once decayed and then became activated showing the commencement of transition. However, these initial disturbances have an effect on the calculated results in the turbulent region [1, 2]. Therefore, we show the following turbulence statistics as ensemble averaged values of several iterations with different initial disturbances.

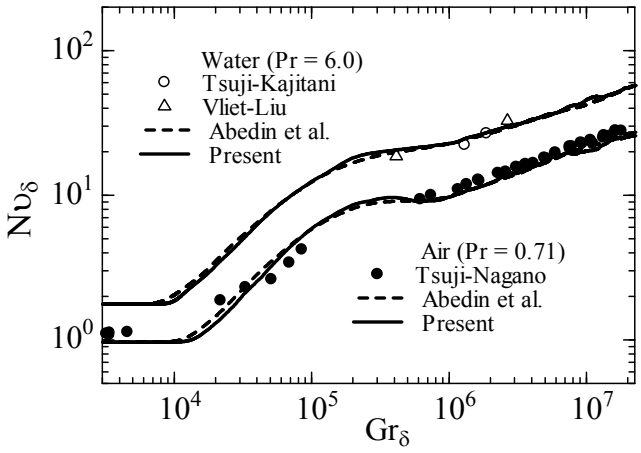

Fig. 2. Code validation - Heat transfer rates in natural-convection boundary layer on length scale δ for air (Pr = 0.71) and water (Pr = 6.0).

3.1. Code validation

The predicted heat transfer rates in the natural-convection boundary layers both in air and water are validated with the analysis of previous investigations. Figure 2 depicts the Nusselt number, Nu_δ against the Grashof number, Gr_δ based on the integral thickness of velocity boundary layer, δ. The predicted heat transfer rates obtained with the disturbance of less than 5% agree completely well with those obtained by the results in the numerical simulations done with the disturbance of less than 1% of Abedin et al. [1] for both air and water. Moreover, the present results of heat transfer rates correspond well with the results obtained by the experimental investigation of Tsuji-Nagano [12] for air and of both Vliet-Liu [8] and Tsuji-Kajitani [18] for water. As the results in the present analysis correspond quantitatively well with those of the established results, therefore, it can be concluded that the present analysis would provide credible findings in the characteristics of boundary layer flows along a heated vertical flat plate.

3.2. Laminar boundary layer flows

3.2.1. Velocity and temperature distributions in the natural-convection boundary layer

The predicted velocity and temperature profiles in the laminar natural-convection boundary layer ($Gr_{\delta_0} = 3000, Re_{\delta_0} = 0$) for air (Pr = 0.71) and water (Pr = 6.0) are shown against y/δ in Figs. 3 (a) and (b), respectively. The dimensionless velocity profile $(u\delta/\nu)/Gr_\delta$ is used in the ordinate in Fig. 3 (a) and the dimensionless temperature profile θ is used in the ordinate in Fig. 3 (b) while the dimensionless distance y/δ is used in the abscissa for both figures. The relation between $(ux/\nu)/Gr_x^{1/2}$ and $(y/x)\ Gr_x^{1/4}$, which is used to express the similarity of the laminar velocity profiles in the space-developing boundary layer [1], is equivalent to the coordinates shown in Fig. 3 (a).

As can be seen from Fig. 3 (a), the velocity profiles for the laminar boundary layer both in air and water are initially zero at the inner boundary layer region and then increase to their respective highest values and finally decrease to zero at the outer boundary layer region. However, the velocity profile for water shows lower peak value compared to that in air due to the effect of high Prandtl number of water. On the other hand, as can be seen from Fig. 3 (b), the temperature profiles both in air and water are initially at their peaks and then decrease to zero. However, at outer boundary layer the profile falls moderately to zero for air and sharply to zero for water. The temperature of the water within the boundary layer becomes ambient at a shorter distance perpendicular to the heated wall compared to that in air due to the effects of higher Prandtl number of water.

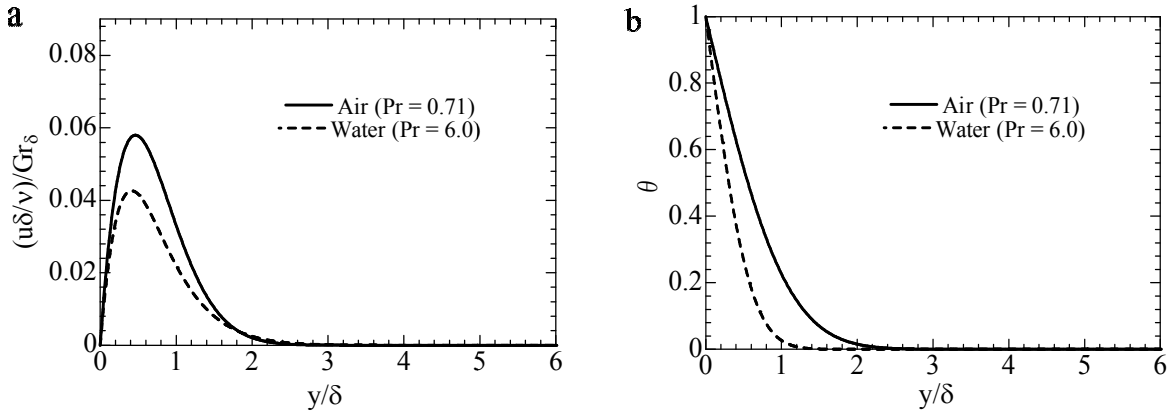

Fig. 3. (a) Velocity profiles; (b) Temperature profiles in laminar natural-convection boundary layer ($\mathrm{Gr}_{\delta_o} = 3000, Re_{\delta_o} = 0$).

3.2.2. Velocity and temperature distributions in the mixed-convection boundary layer

The predicted velocity and temperature profiles in the laminar mixed-convection boundary layer with aiding flow ($\mathrm{Gr}_{\delta_o} = 3000, \mathrm{Re}_{\delta_o} = 3000$) and opposing flow ($\mathrm{Gr}_{\delta_o} = 3000, \mathrm{Re}_{\delta_o} = -3000$) for air (Pr = 0.71) and water (Pr = 6.0) are shown against y/δ in Figs. 4 (a) and (b), respectively. In these figures, the dimensionless velocity profile $(u\delta/\nu)/(B^2\mathrm{Gr}_\delta + \mathrm{Re}_\delta)$ is used in the ordinate while the dimensionless distance y/δ is used in the abscissa. The notation B is a constant used to clarify the characteristics of the integral thickness of the laminar boundary layer flows [2].

As can be seen from Fig. 4 (a), the velocity profiles for the laminar boundary layer both in air and water are initially zero and then increase to their respective peak values, then decrease slightly and finally become constant in the outer boundary layer region due to the aiding flow applied opposite to the gravity. On the other hand, as can be seen from Fig. 4 (b), the velocity profiles both in air and water are initially zero, then increase slightly followed by a sharp drop to their negative constant values in the outer boundary layer region due to the opposing flow applied along the direction of the gravity. However, the velocity profile of water exhibits lower values throughout the boundary layer compared to that in air due to the effect of higher Prandtl number.

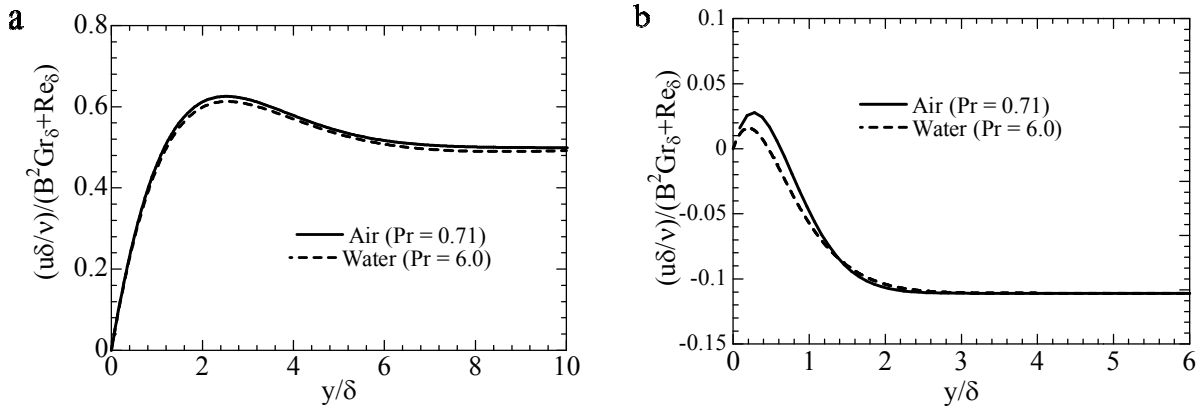

Fig. 4. Velocity profiles in laminar mixed-convection boundary layers with (a) aiding flow ($\mathrm{Gr}_{\delta_o} = 3000, \mathrm{Re}_{\delta_o} = 3000$); (b) with opposing flow ($\mathrm{Gr}_{\delta_o} = 3000, \mathrm{Re}_{\delta_o} = -3000$).

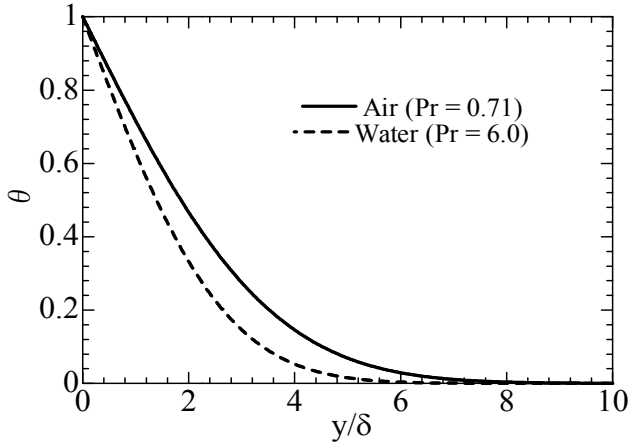

Fig. 5. Temperature profiles in laminar mixed-convection boundary layers with aiding flow ($Gr_{\delta_0} = 3000, Re_{\delta_0} = 3000$).

The predicted temperature profiles in the laminar mixed-convection boundary layer with aiding flow ($Gr_{\delta_0} = 3000, Re_{\delta_0} = 3000$) for air (Pr = 0.71) and water (Pr = 6.0) are shown against y/δ in Fig. 5. As can be seen from the figure, the temperature profiles both in air and water are initially at their peaks and then decrease to zero with water reaching zero level at a shorter distance perpendicular to the heated wall compared to air due to the effects of higher Prandtl number of water. The temperature profiles for opposing flow both in air and water exhibits the similar behaviours as those in aiding flow (not shown in figures).

3.3. Transition boundary layer flows

3.3.1. Velocity and temperature distributions in the natural-convection boundary layer

The predicted mean velocity and temperature profiles from laminar to turbulence in natural-convection boundary layer ($Gr_{\delta_0} = 3000, Re_{\delta_0} = 0$) in air (Pr = 0.71) are shown against y/δ_0 in Figs. 6 (a) and (b), respectively. The dimensionless velocity profile u/U_0 is used in the ordinate of Fig. 6 (a) and the dimensionless temperature θ is used in the ordinate of Fig. 6 (b), while the dimensionless distance y/δ_0 is used in the abscissa in both cases.

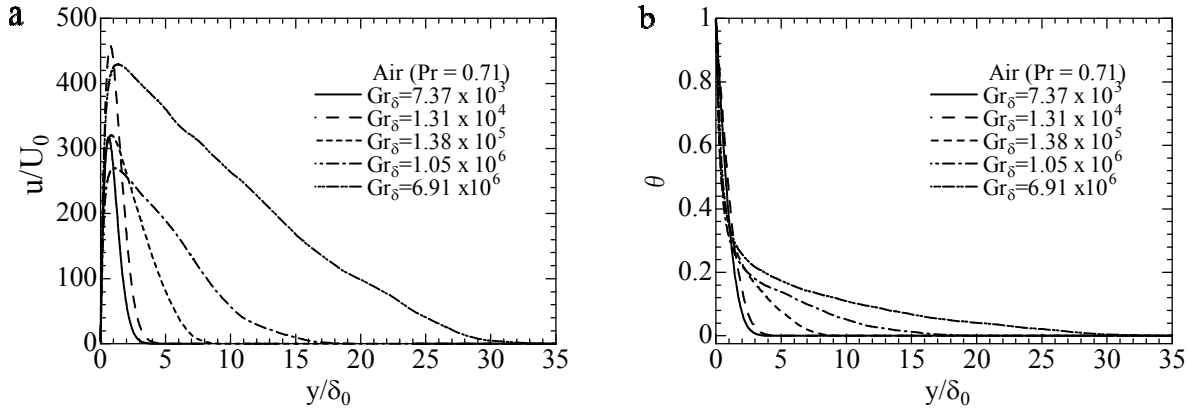

Fig. 6. (a) Mean velocity; (b) temperature profiles from laminar to turbulence in natural-convection boundary layer ($Gr_{\delta_0} = 3000, Re_{\delta_0} = 0$).

As can be seen in Fig. 6 (a), the velocity profiles from laminar to turbulence ($Gr_\delta = 7.37\times10^3 \sim 6.91\times10^6$) in air are initially zero, then increase to their respective peak values and finally decreases to zero at the outer boundary layer region. It is also observed that the magnitudes of the velocity profile increase to their peaks and show wider span in the distributions with an increase in the Grashof number Gr_δ. This is due to the increasing trend in the velocity within the growing boundary layer thickness. The velocity profiles in water show similar behaviours with lower peaks and less wider span in the distribution (not shown in figure).

On the other hand, as can be seen in Fig. 6 (b), the temperature profiles in air are initially at the peak and then decrease moderately to zero. The temperature profiles in water show similar behaviors with sharp falling in the outer boundary layer region (not shown in figure).

3.3.2. Velocity and temperature distributions in the mixed-convection boundary layer

The predicted mean velocity and mean temperature profiles from laminar to turbulence in mixed-convection boundary layers with aiding flow ($Gr_{\delta_0} = 3000, Re_{\delta_0} = 300$) in air (Pr = 0.71) are shown against y/δ_0 in Figs. 7 (a) and (b), respectively.

As can be seen in Fig. 7 (a), the velocity profiles from laminar to turbulence ($Gr_\delta = 6.23\times10^3 \sim 2.31\times10^6$) in air are initially zero, then increase to their respective peak values and finally decrease to a constant positive value due to the aiding flow opposite to the gravity. It is also observed that the magnitude of the velocity profile increases to their peaks and shows wider span in the distributions with an increase in the Grashof number Gr_δ. This is due to the increasing trend in the velocity within the developing boundary layer thickness as specified above. The velocity profiles in water show similar behaviours with lower peaks and less wider span in the distribution (not shown in figure).

On the other hand, as can be seen in Fig. 7 (b), the temperature profiles in air are initially at the peak and then decrease moderately to zero. The temperature profiles in water show similar behaviors with sharp falling in the outer boundary layer region (not shown in figure).

4. Conclusions

A numerical investigation is carried out in the natural- and mixed-convection boundary layer flows both in air and water along a heated vertical flat plate by time-developing DNS in order to clarify the effects of the freestream velocity and Prandtl number on the boundary layer flows. The predicted results of heat transfer rates in the natural-

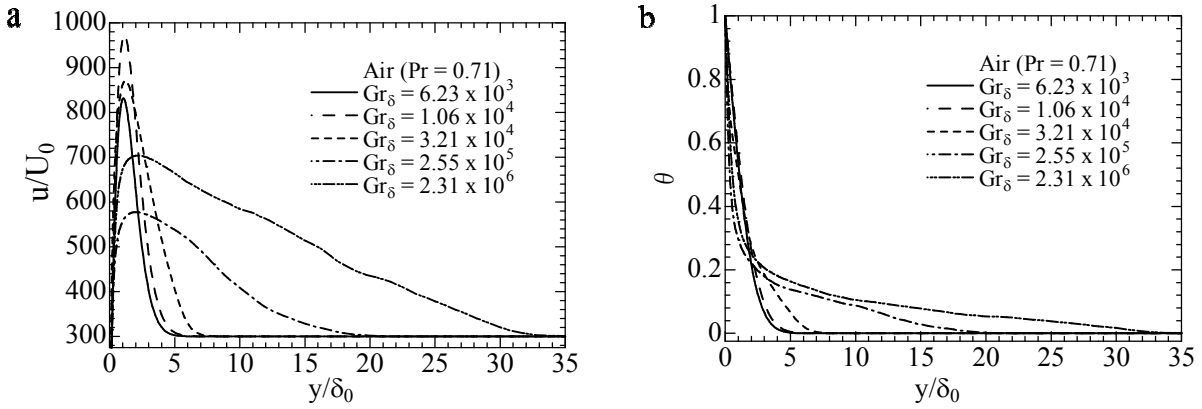

Fig. 7. (a) Mean velocity; (b) mean temperature profiles from laminar to turbulence in mixed- convection boundary layer with aiding flow ($Gr_{\delta_0} = 3000, Re_{\delta_0} = 300$).

convection boundary layers both in air and water have been well compared and validated with the existing observations.

The following conclusions may be drawn from the present analysis:

- In the laminar natural-convection boundary layer both in air and water, the velocity profiles are initially zero in the inner boundary layer region and then increase to their respective highest values and finally decrease to zero at the outer boundary layer region. However, the velocity profile of water shows lower peak value compared to that in air due to the effect of higher Prandtl number. On the other hand, the temperature profiles both in air and water are initially at their peak values and finally decrease to zero. Moreover, the temperature profile in water within the boundary layer becomes ambient at a shorter distance perpendicular to the heated wall compared to that in air due to the effects of higher Prandtl number of water.
- In the laminar mixed-convection boundary layer with aiding flow both in air and water, the velocity profiles are initially zero and then increase to the peak at certain level and then decreases to the constant positive values in the outer boundary layer region. Furthermore, the velocity profile of water exhibits lower values throughout the boundary layer compared to that in air. In the case of opposing flows both in air and water, the velocity profiles finally show a sharp drop to a constant negative value in the outer boundary layer region. On the other hand, the temperature profiles both in air and water show the similar behaviors with those observed in the flow of natural-convection.
- For the transition natural-convection boundary layer in air, the velocity profiles are initially zero and then increase to their respective peak values and finally decreases to zero level. The magnitude of the velocity profile increases with an increase in Grashof number due to the increasing trend in the boundary layer thickness. On the other hand, the temperature profiles both in air and water are initially at the peak and then decrease to zero analogous to those in the laminar flows.
- The velocity and temperature profiles in the transition mixed-convection boundary layer with aiding flow in air show the similar behaviors compared to the profiles observed in the natural-convection boundary layer.

Acknowledgements

The authors would like to acknowledge Professor Toshihiru Tsuji, Nagoya Institute of Technology, Japan, for his invaluable suggestions and great assistances in the time of simulation and experimentation.

References

[1] M. Z. Abedin, T. Tsuji, Y. Hattori, Direct numerical simulation for a time-developing natural-convection boundary layer along a vertical flat plate, Int. J. Heat Mass Transfer, 52(19-20) (2009) 4525-4534.
[2] M. Z. Abedin, T. Tsuji, Y. Hattori, Direct numerical simulation for a time-developing combined-convection boundary layer along a vertical flat plate, Int. J. Heat Mass Transfer, 53(9-10) (2010) 2113-2122.
[3] M. Z. Abedin, T. Tsuji, Effect of freestream on thermally-driven boundary layers along a heated vertical flat plate, in: Proc. 14th Int. Heat Transfer Conf., Washington D.C., USA, TRK-20 of CD-ROM, 2010, pp. 1-8.
[4] M. Z. Abedin, T. Tsuji, Structural characteristics of turbulent combined-convection boundary layers along a vertical flat plate, in: Proc, 7th Int. Conf. On Heat Transfer, Fluid Mechanics And Thermodynamics, Antalya, Turkey, CD-ROM of HEFAT 2010, 2010, pp. 2175-2180.
[5] M. Z. Abedin, T. Tsuji, Transition behavior and turbulence characteristics in combined-convection boundary layers along a heated vertical flat plate, in: Proc. 13 Asian Congress Fluid Mechanics, Dhaka, Bangladesh, 2010, pp. 759-762.
[6] M. Z. Abedin, T. Tsuji, J. Lee, Effects of freestream on transition behaviors and turbulence characteristics of thermally-driven boundary layers along a heated vertical flat plate, Int. J. Heat Fluid Flow, 36 (2012) 92-100.
[7] M. Z. Abedin, T. Tsuji, J. Lee, Turbulence characteristics and vortical structures in combined-convection boundary layers along a heated vertical flat plate, Int. J. Heat Mass Transfer, 55(15-16) (2012) 3995-4002.
[8] G. C. Vliet, C. K. Liu, An experimental study of turbulent natural convection boundary layers, Trans. ASME J. Heat Transfer, C-91 (1969) 517-531.
[9] T. Fujii, M. Takeuchi, M. Fujii, K. Suzaki, H. Uehara, Experiment on natural-convection heat transfer from the outer surface of a vertical cylinder to liquids, Int. J. Heat Mass Transfer, 13 (1970) 753-587.
[10] M. Miyamoto, H. Kojino, J. Kurima, I. Takanami, Development of turbulence characteristics in a vertical free convection boundary layer, in: Proc. 7th Int. Heat Transfer Conf., F.R.G., Munich, 2, 1982, pp. 323-328.
[11] K. Kitamura, T. Inagaki, Turbulent heat and momentum transfer of combined forced and natural convection along a vertical flat plate -

aiding flow, Int. J. Heat Mass Transfer, 30(1) (1987) 23-41.
[12] T. Tsuji, Y. Nagano, Characteristics of a turbulent natural convection boundary layer along a vertical flat plate, Int. J. Heat Mass Transfer, 31(8) (1988) 1723-1734.
[13] T. Tsuji, Y. Nagano, Turbulence measurements in a natural convection boundary layer along a vertical flat plate, Int. J. Heat Mass Transfer, 31(10) (1988) 2101-2111.
[14] T. Tsuji, Y. Nagano, Velocity and temperature measurements in a natural convection boundary layer along a vertical flat plate, Exp. Therm. Fluid Sci. 2 (1989) 208-215.
[15] T. Tsuji, Y. Nagano, M. Tagawa, Thermally driven turbulent boundary layer, in: Proc. 8th Symposium on Turbulent Shear Flows, Munich, 1, 1991, pp. 24.3.1-24.3.6.
[16] T. Tsuji, Y. Nagano, M. Tagawa, Experiment on spatial and temporal turbulent structures of a natural convection boundary layer, Trans. ASME J. Heat Transfer, 138 (1992) 19-26.
[17] T. Tsuji, Y. Nagano, Structural characteristics of a turbulent natural convection boundary layer, in: Proc. 2nd China-Japan Work Shop Turbulent Flows, 1996, pp. 277-289.
[18] T. Tsuji, T. Kajitani, Turbulence characteristics and heat transfer enhancement of a natural convection boundary layer in water along a vertical flat plate, in: Proc. 13th Int. Heat Transfer Conf., Sydney, TRB-08 of CD-ROM, 2006.
[19] W. M. To, J. A. C. Humphrey, Numerical simulation of buoyant, turbulent flow-1. Free convection along a heated, vertical flat plate, Int. J. Heat Mass Transfer, 29(4) (1986) 573-5926.
[20] R. A. W. M. Henkes, C. J. Hoogendoorn, Comparison of turbulence models for the natural convection boundary layer along a heated vertical plate, Int. J. Heat Mass Transfer, 32(1) (1989) 157-169.
[21] T. W. J. Peeters, R. A. W. M. Henkes, The Reynolds-stress model of turbulence applied to the natural convection boundary layer along a heated vertical plate, Int. J. Heat Mass Transfer, 35(2) (1992) 403-420.
[22] M. J. Watts, C. T. Chou, Mixed convection heat transfer to supercritical pressure water, in: Proc. 7th Int. Heat Transfer Conf., 3(MC16), 1982, pp. 495-500.
[23] J. Wang, J. Li, J. D. Jackson, A study of the influence of buoyancy on turbulent flow in a vertical plane passage, Int. J. Heat Fluid Flow, 25(3) (2004) 420-430.
[24] N. Kasagi, M. Nishimura, Direct numerical simulation of combined forced and natural turbulent convection in a vertical plane channel, Int. J. Heat Fluid Flow, 18(1) (1997) 88-99.
[25] Y. Hattori, T. Tsuji, Y. Nagano, N. Tanaka, Characteristics of turbulent combined-convection boundary layer along a vertical heated plate, Int. J. Heat Fluid Flow, 21(5) (2000) 520-525.
[26] Y. Hattori, Turbulent characteristics and transition behavior of combined-convection boundary layer along a vertical heated plate, Ph.D. Thesis, Nagoya Institute of Technology, (2001).
[27] Y. Hattori, T. Tsuji, Y. Nagano, N. Tanaka, Effects of freestream on turbulent combined-convection boundary layer along a vertical heated plate, Int. J. Heat Fluid Flow, 22(3) (2001) 315-322.
[28] T. Inagaki, K. Kitamura, Turbulent heat transfer of combined forced and natural convection along a vertical flat plate (Opposing flow), Trans. JSME, B 54(499) (1988) 675-680. (In Japanese)
[29] T. Inagaki, K. Kitamura, Turbulent heat transfer of combined forced and natural convection along a vertical flat plate (Effect of Prandtl number), Trans. JSME, B 54(505) (1988) 2515-2522. (In Japanese)

Available online at www.sciencedirect.com

ScienceDirect

Procedia Engineering00 (2015) 000–000

Procedia Engineering

www.elsevier.com/locate/procedia

6th BSME International Conference on Thermal Engineering (ICTE 2014)

Numerical investigation of effect of Mach number over backward facing step

Konica Sarker [a]*, Mohammad Ali [b] , Quamrul Islam [b]

[a] Bangladesh Power Development Board, Dhaka, Bangladesh.

[b] Department of Mechanical Engineering, BUET, Dhaka-1000, Bangladesh

Abstract

A numerical study has been carried out to investigate the flow field characteristics of a transonic compressible flow over a flat plate with backward facing step. The study has been performed by solving Two-Dimensional Navier-Stokes equations. The system of governing equations has been solved, using an explicit Harten-Yee Non- MUSCL Modified flux type TVD scheme and a zero-equation algebraic turbulence model to calculate the eddy viscosity coefficient. The results presented in this paper are computed for fixed step height, h=7.5 mm and for different Mach numbers, M= 0.8, 1.0 1nd 1.2. The details on pressure, temperature and velocity field, together with recirculation length, expansion shock, reattached shock, interaction of shock wave are reported. The variations of flow field characteristics due to change of Mach number are also presented.

Peer-review under responsibility of organizing committee of the 6th BSMEInternational Conference on Thermal Engineering (ICTE 2014).

*Keywords:*Mach number; backward step;recirculation;

Introduction:

The increasing interest in high speed flow has promoted more research in the area of boundary layer transition. Transition of boundary layer, separation and reattachment of flow are strongly influenced by any imperfections that exit on aerodynamic surfaces. These imperfections, or roughness elements, can occur in various forms and are of different sizes. They may include regions of waviness, bulges, steps, gaps at junctions, surface contamination from insect debris, ice and dirt particles of various sorts. Although, modern manufacturing and maintenance procedures

* Corresponding author. Tel.: +8801717743598; fax: +0-000-000-0000 .
*E-mail address:*konica_eng@yahoo.com

Peer-review under responsibility of organizing committee of the 6th BSME International Conference on Thermal Engineering (ICTE 2014).

make it possible to provide reasonable good operational surfaces, some imperfections are unavoidable, particularly those arising from such things as the installation of imperfection panels. They often arise in the form of sharp-edged steps. Supersonic compressible flow over a flat plate with steps (both forward facing and backward facing) is very important in many engineering applications. In present works a high speed flow field on flat plate with facing steps is considered.

Chen et al. [1] and Scherberg [2] investigated the flow field for different Mach number with a fixed step height. Chen et al. showed the flow structures, including supersonic laminar boundary layer, separation, reattachment, redeveloping turbulent boundary layer, expansion wave fan and reattachment shock in the transient flow fields. Again Scherberg presented that the pressure changes from free stream pressure to base pressure were linear functions of free stream pressure for each Mach speed and step height. Popusco and Panait [3] conducted an experimental study to analyze the field velocity of a fully developed turbulent incompressible flow behind a backward facing step with a curve nose shape. Al-Maaitah et al. [4] investigated the effect of suction on the stability of compressible flow. Yang et al. [5] show the effect of the incoming boundary layer, step height and inlet free stream Mach number on the flow characteristics. Crouch et al. [6] reported on the boundary layer displacement thickness due to stepping. Through a considerable number of researchers carried out their researches on flow over a flat plate, still it faces many unsolved problems. So more investigations are required to flow over a flat plate and overcome those problems. The physics of flow separation, flow transition from subsonic to supersonic and dynamical behavior of the flow field are addressed for different Mach number. It is expected that the results of this investigation would be a useful guide to the effect of different Mach number on various flow field characteristics.

Nomenclature

C_p	Specific heat at constant pressure	J/(kg.K)
E	Total energy	J/m^3
$\hat{F}$	Transform flux vector in ξ -direction	
G	Flux vector in y-direction	
P	Pressure	Pa
P_{in}	Inlet Pressure	Pa
R	Universal gas constant	J/(kg.mol.K)
T	Temperature	K
U	Vector in conservative variables	
$\hat{U}$	Transformed vector in conservative variables	
ρ	Mass density	kg/m^3
$\sigma_{x,y}$	Normal stress	Pa
τ	Shear stress	Pa
μ	Coefficient of dynamic viscosity	Kg/(m.s)
κ	Thermal conductivity	W/(m.K)
ν	Viscous term	

2. Mathematical Description:

The flow field is governed by the unsteady, two-dimensional full Navier-Stokes and species continuity equations. The body forces are neglected. With the conservation-law form, these equations can be expressed by

$$\frac{\partial U}{\partial t}+\frac{\partial F}{\partial x}+\frac{\partial G}{\partial y}=\frac{\partial F_v}{\partial x}+\frac{\partial G_v}{\partial y}$$

Where $U=\begin{pmatrix}\rho\\ \rho u\\ \rho v\\ E\end{pmatrix}$, $F=\begin{pmatrix}\rho u\\ \rho u^2+p\\ \rho uv\\ (E+p)u\end{pmatrix}$, $G=\begin{pmatrix}\rho u\\ \rho uv\\ \rho u^2+p\\ (E+p)v\end{pmatrix}$, $F_v=\begin{pmatrix}0\\ \sigma_x\\ \tau_{xy}\\ \sigma_x u+\tau_{yx}v-q_x\end{pmatrix}$, $G_v=\begin{pmatrix}0\\ \tau_{yx}\\ \sigma_y\\ \tau_{xy}u+\sigma_{yv}-q_y\end{pmatrix}$

, $\mathrm{P}=\sum_{i=1}^{ns}\rho_i R_i T=\sum_{i=1}^{ns}\rho_i\frac{R}{W_i}T$

$$E=\sum_{i=1}^{ns}\rho_i h_i-\sum_{i=1}^{ns}\rho_i\frac{R}{W_i}T+\frac{\rho}{2}(u^2+v^2)=\sum_{i=1}^{ns}\rho_i C_{pi}T-\sum_{i=1}^{ns}\rho_i\frac{R}{W_i}T+\frac{\rho}{2}\left(u^2+v^2\right)$$

$$\sigma_x=\lambda\left(\frac{\partial u}{\partial x}+\frac{\partial v}{\partial y}\right)+2\mu\left(\frac{\partial u}{\partial x}\right),\ \sigma_y=\lambda\left(\frac{\partial u}{\partial x}+\frac{\partial v}{\partial y}\right)+2\mu\left(\frac{\partial v}{\partial y}\right),\tau_{xy}=\tau_{xy}=\mu\left(\frac{\partial u}{\partial y}+\frac{\partial v}{\partial x}\right),\lambda=-\frac{2}{3}\mu$$

3. Flow Field Description and Numerical Parameters:

The geometric configuration of the calculation domain is shown in Fig. 1. The domain dimension in the stream wise horizontal and vertical directions are L= 10 cm and H= 5 cm, respectively. Facing step is located at the inlet (left) boundary of the calculation domain. Throughout the study, the grid system consists of 194 nodes in the longitudinal direction and 121 nodes in the transverse direction. The grids are clustered near the wall.

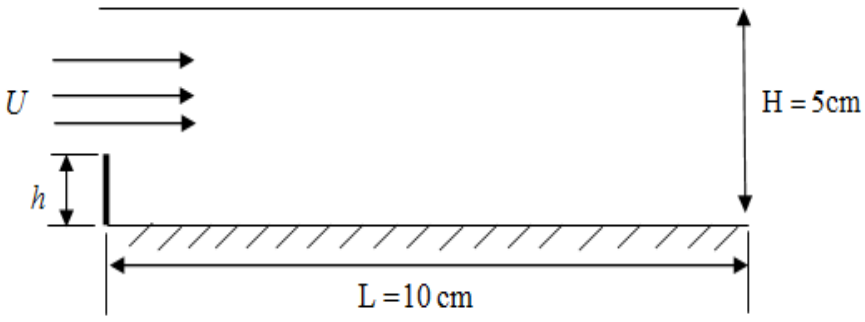

Fig.1 Calculation domain

4. Results and Discussion:

The main objective of this study is to investigation the variation of different flow field characteristics of a flow having Mach no 0.8, 1.0 and 1.2 of step height 7.5 mm. The investigation has been done by varying the mach numbers at constant step height of 7.5mm. The calculated results are presented in terms of velocity, Mach, pressure and temperature contour. Results with varying parameters are to be analyzed and discussed under the following contexts: *(i) Different shocks characteristics (ii) Dynamical behavior of the flow field and (iii) Effect of pressure and temperature.*

4.1 Different shocks characteristics:

Figures 2-4 illustrate the Mach contour for different Mach numbers. Mack contours are characterized by the presence of shocks in the flow. The two shock regions are visible in the flow field, namely corner expansion shock and reattachment shock. Expansion shock appears to emanate from the vicinity of the top of the step and reattached shock appears at the reattachment region, which is located below the expansion shock region. By analyzing the figures, it is found that, the expansion shock rotates clockwise, moves downward and the angle of shock with main flow direction decreases with the increase of Mack number. Due to the change of Mach number, the width of the expansion shock and the degree of expansion decreases. An interaction of two shocks (expansion shock and reattachment shock) is found in the flow field and its position also rotates with the increase of Mach number.

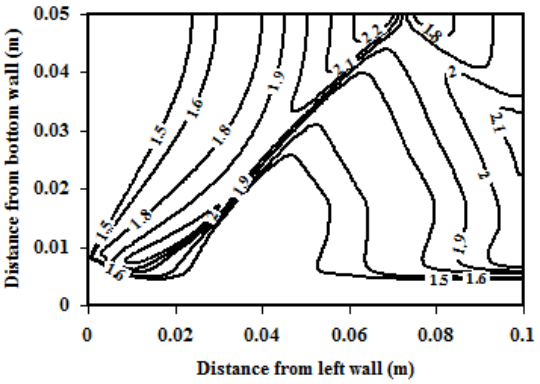

Fig.2 M/M_{in} contour for M= 0.8

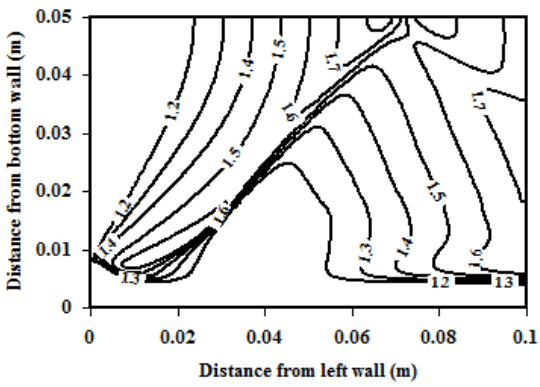

Fig. 3 M/M_{in} contour for M= 1.0

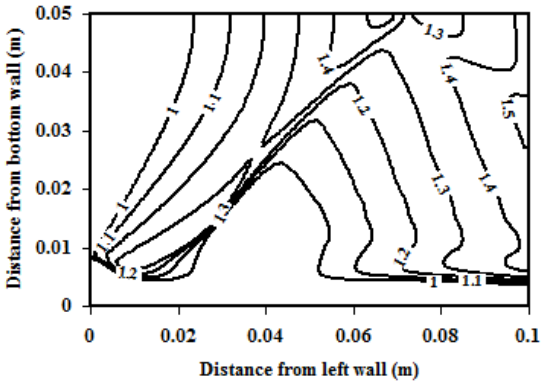

Fig. 4 M/M_{in} contour for M= 1.2

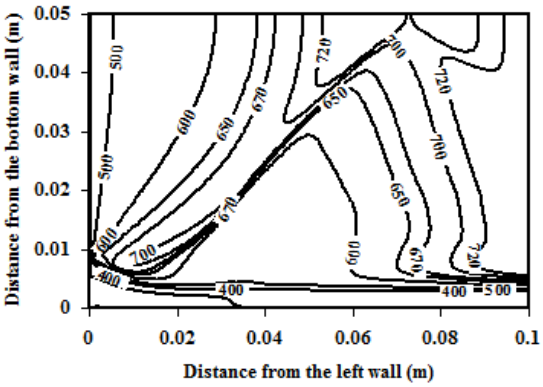

Fig.5 Stream wise Velocity contour for M=1.0

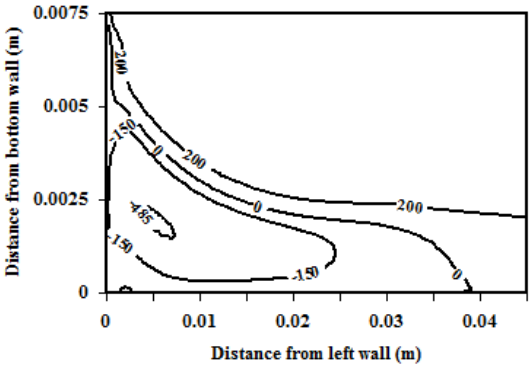

Fig. 6 Recirculation zone for M= 0.8

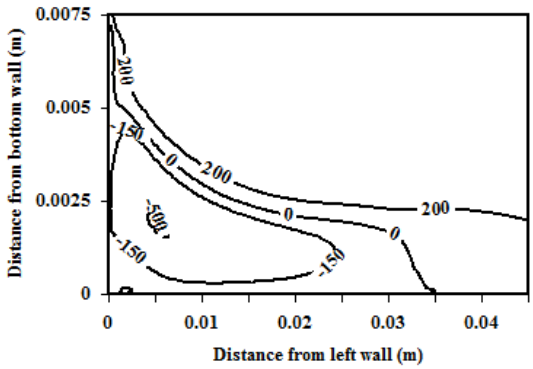

Fig.7 Recirculation zone for M= 1.0

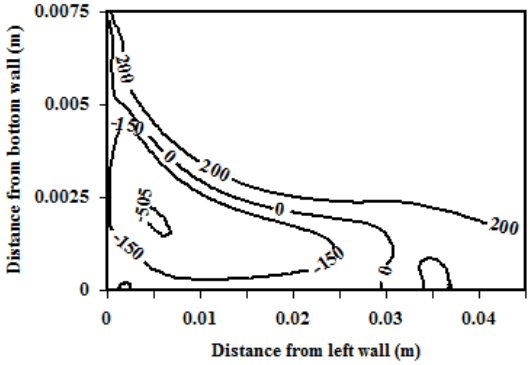

Fig. 8 Recirculation zone for M= 1.2

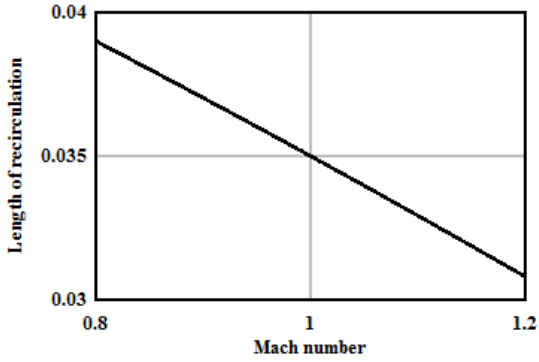

Fig.9 Recirculation length for different Mach Numbers

4.2 Dynamical behaviour of the flow field:

The velocity contours are characterized by the sudden rise of velocity in the expansion shock region (in Fig.5) and it decreases at reattachment shock region. In the flow field, it is found that after the interaction of two shocks a part of flow is reflected to the downward direction which exists up to the exit of the boundary (Fig. 5). At the left bottom corner of the velocity field recirculation appears and the zero value of the velocity contour is considered as recirculation zone. The length of this zone along the bottom wall is considered as recirculation length. Figures 6-8 show the recirculation zone for different Mach number. For close observation the figures are magnified and shown partly by height of 7.5 mm (from bottom wall) and length of 45 mm (from left boundary). With the increase of Mach number, the length of recirculation decreases, which is found, 0.039, 0.035 and 0.0308 m respectively. From fig. 9 it is found that, for all cases, recirculation length decreases linearly with the increase of Mach number. This is caused by the high compression of inlet flow for higher Mach number. But the strength of recirculation i.e the turbulence excited in this case becomes stronger, as the change of Mach number. The stream wise vorticity is stronger near the step and reduces in strength further downstream. The maximum strength of recirculation is found at about one-fourth of the recirculation length.

Figures 10-11 show the transverse velocity contours. Apart from the inlet, the maximum and minimum value of transverse wise velocity is located immediately after the tips of the step. The minimum value of the transverse velocity immediately after the tip physically demands that the flow needs some stream wise distance to adjust and become fully developed. Due to the change of Mach number, there occurs a little increase in area of realm where maximum and minimum cross-stream velocity demanding to get fully developed.

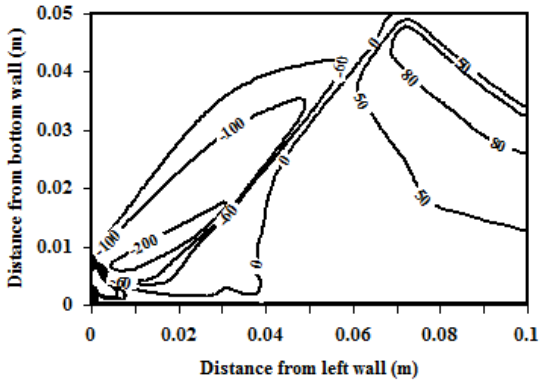

Fig.10Transverse velocity contour for M= 0.8

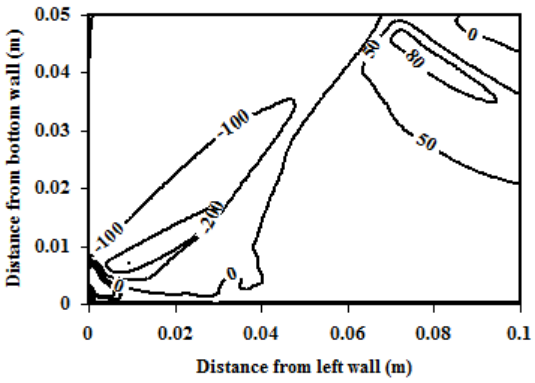

Fig.11 Transverse velocity contour for M= 1.2

4.3 Effect on Pressure and Temperature in the flow Field:

Figures 12-13 represent pressure contour for different Mach number. The pressure contours show a sudden drop of pressure in the corner expansion shock region and immediate behind the expansion shock, the reattachment shock evolves where the pressure again increases. The minimum pressure is found in the recirculation zone. Actually this low pressure zone triggers the flow to generate recirculation. A little increase of pressure is in the expansion shock region, reattached shock region, along the step height and recirculation zone, as the Mach number increases. The striking pressure increases, with the increase of Mach numbers and the position moves to the left.

From the temperature contour as shown in Fig. 14-15, it is found that there is a sudden drop of temperature in the corner expansion shock region and again the temperature gradually increases at reattachment shock region. There is a sudden increase of temperature near the step because of recirculation zone, which tends to accumulate the recirculated particles near the left-bottom corner causing the increasing of temperature. The maximum temperature in this region can be found around 940K. There is no remarkable change of temperature in the flow field, as the change of Mach number.

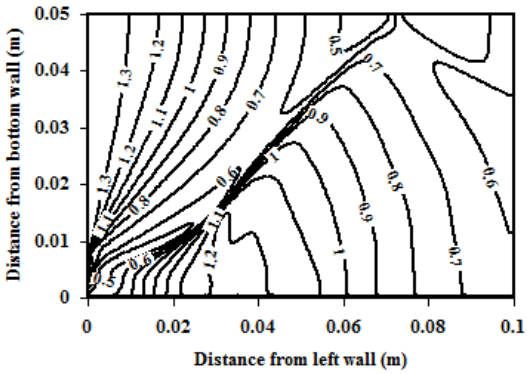

Fig.12 P/P_{in} contour for Mach number 0.8

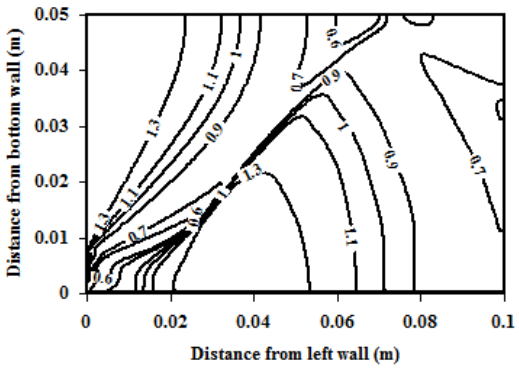

Fig. 13 P/P_{in} contour for Mach number 1.2

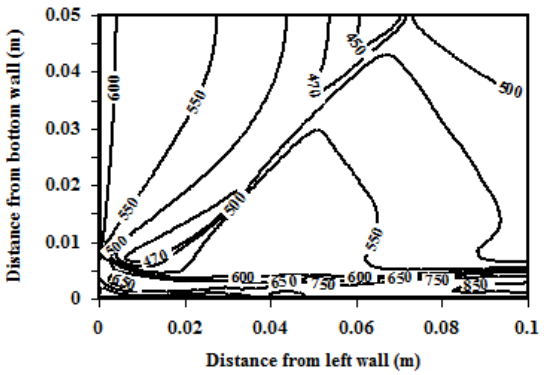

Fig. 14 Temperature contour for Mach number 0.8

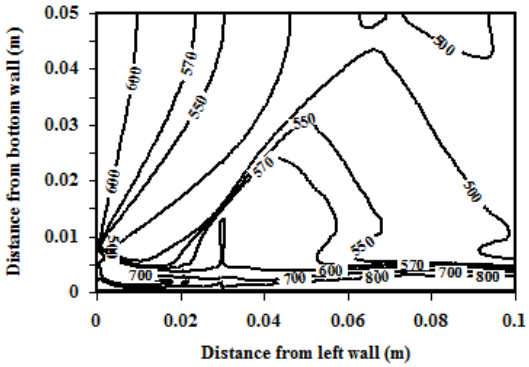

Fig. 15 Temperature contour for Mach number 1.2

5. Conclusion:

A study of transonic flow over a backward facing step is carried out by using an explicit Harten-Yee Non- MUSCL Modified flux type TVD scheme. The effects of Mach number on the dynamical behaviour of flow field have been reported. A corner expansion shock, emanate from the vicinity of the top of the step; reattached shock, below the expansion shock region; and interaction of this two shocks; recirculation zone, immediate behind the step and their characteristics are the major findings of the flow field addressed herein. Sudden drop of pressure and temperature in expansion shock region can be observed. At the end of the recirculation, the reattachment shock follows the expansion shock where both the pressure and temperature again increase. With the increase of Mach number, the corner expansion shock and the interaction position of two shocks rotate clockwise, move downward and the angle of shock with main flow direction decreases. The degree of expansion at expansion shock region, the width of the expansion shock and length of recirculation decrease, with the increase of Mach number. But the strength of recirculation increases in this condition. Maximum temperature and minimum pressure of the flow field are found in recirculation zone, which is almost same for different Mach numbers.

Acknowledgements

The authors are sincerely thankful to Bangladesh University of Engineering and Technology, Dhaka-1000, Bangladesh, for supporting this work.

References:

[1] Scherberg, M. G. and Smith, H. E. “An experimental study of supersonic flow over a rearward facing step”, AIAA Journal, Vol-5, no-1, January 1967, pp. 51-56.

[2] Chen Z., Yi S.H., Tian L.F, He L., Zhu Y.Z., “Flow visualization of supersonic laminar flow over a backward-facing step via NPLS”, Journal of shock wave, Issue 4, Volume 23, July 2013, pp. 299-306.

[3] Popusco, F. and Panait, T. “Numerical modelling and experimental validation of a turbulent separated reattached flow”, International Journal of Mathematical Models and Methods in Applied Science, Issue-4, Volume-1, 2007, pp.280-284.

[4] Al-Maaitah, A. A., Nayfeh, A. H. and Ragab, S. A., “Effect of Suction on the stability of Subsonic Flows over Smooth Backward-Facing Steps”, AIAA Journal, Vol-28, No-11, pp. 1916.

[5] Yang, A. S., Hsieh, W. H. and Kuo, K. K., “Theoretical Study of Supersonic Flow Separation over a Rearward-Facing Step” 27th Joint Propulsion Conference (1991), 24 June 1991 - 26 June 1991.

[6] Crouch, J.D., Kosorygin, V.S. and Ng L.L, "Modelling the Effect of Steps on Boundary Layer Transition”, Fluid mechanics and its Application, Volume 78, 2006, pp. 37-44.

Modified Norris–Reynolds One–Equation Model

M. M. Rahman[1], *A. K. M. Sadrul Islam*[2], *M. J. Lampinen*[1] *and T. Siikonen*[1]

[1]Aalto University School of Engineering, P.O. Box 14400, FI–00076 AALTO, Finland

[2]Department of Mechanical & Chemical Engineering,

Islamic University of Technology, Board Bazar, Gazipur 1704, Bangladesh

[1]E-mail: Mizanur.Rahman@aalto.fi

Abstract

A modified version of Norris–Reynolds (NR) k–equation turbulence model is proposed to account for the distinct effects of low–Reynolds number (LRN) and wall proximity. The turbulent kinetic energy k and the dissipation rate ϱ are evaluated using the k–transport equation in conjunction with the Bradshaw and other empirical relations. The eddy–viscosity formulation maintains the positivity of normal Reynolds stresses and preserves the anisotropic characteristics of turbulence in the sense that they are sensitized to rotational and non–equilibrium flows. The modified NR (MNR) model is validated against well–documented flow cases yielding predictions in good agreement with the direct numerical simulation (DNS) and experimental data. Comparisons indicate that the MNR model offers some improvement over the original NR model and competitiveness with the Spalart–Allmaras one–equation model.

Keywords: One–equation model, turbulence anisotropy, two–layer model, non–equilibrium flow.

Available online at www.sciencedirect.com

ScienceDirect

Procedia Engineering00 (2015) 000–000

Procedia Engineering

www.elsevier.com/locate/procedia

6th BSME International Conference on Thermal Engineering (ICTE 2014)

Physics of supersonic mixing in parallel and non-parallel streams passing over base thickness

Mohammad Ali*, TAGMZN Jubery, Sanchita Amin, M Quamrul Islam

Department of Mechanical Engineering, Bangladesh University of Engg. and Technology
Dhaka – 1000, Bangladesh

Abstract

The mixing flow field of two-parallel and non parallel gaseous streams has been studied numerically. The streams are of air and hydrogen and come into contact after passing over a finite thickness base. The two gas streams are delivered from a high-pressure reservoir and entering into the domain with atmospheric pressure. The two-dimensional unsteady Navier-Stokes equations, energy, mass diffusion and species continuity equations are numerically simulated to analyze the mixing layer in supersonic flow field. An explicit Harten-Yee Non-MUSCL Modified flux-type TVD (total variation diminishing) scheme is used to solve the system of equations. An algebraic turbulence model is used to calculate the eddy viscosity coefficient. Keeping constant the inlet pressure and velocity of the streams, the merging angle is varied to observe the physics of flow fields, mixing of two-streams and mixing efficiency. The results show that the increase of merging angle causes stronger interactions between two streams, high momentum exchange and eventually enhancement of mixing between two streams.

Peer-review under responsibility of organizing committee of the 6th BSMEInternational Conference on Thermal Engineering (ICTE 2014).

Keywords: Supersonic combustor, mixing, shear layers, merging angle;

1. Introduction

Turbulent mixing layers occur in flow fields of many engineering applications e.g., combustion chambers, pre-mixers for gas turbine combustors, chemical lasers, propulsion systems and flow reactors. Particularly, the mixing of reactants and their complete combustion in supersonic combustion ramjet (scramjet) engines has drawn special

* Corresponding author. Tel.: +88-01732194776; fax: +88-02-8613046.
E-mail address: mali@me.buet.ac.bd

Peer-review under responsibility of organizing committee of the 6th BSME International Conference on Thermal Engineering (ICTE 2014).

attention of present scientists. In supersonic combustion systems, the flow speeds are so high that the fuel and oxidizer have little time to mix. The shear layers are naturally unstable and usually lead to a large scale mixing. The higher the Mach number, the longer length it takes for the shear layers to become unstable. This reduces mixing accomplished in a given length. Several configurations of combustor have been studied to seek the enhancement of mixing. Generally parallel, normal or oblique type mixing are used and the most of the researchers carried out their study on two parallel supersonic streams and in all the cases parameters, like density ratio, pressure ratio, merging angles etc. can affect on the penetration and mixing efficiency.

Guirguis et al. [1] performed two-dimensional time-dependent numerical simulation of the convective mixing of two supersonic parallel streams of air. They simulated a supersonic shear layer in a two dimensional channel of 20 cm long and 2.4 cm high and used flux corrected transport algorithm neglecting all diffusion transport processes. Comparisons were made for the vorticity, density and pressure contour of confined and unconfined shear layer. Farouk et al. [2] performed numerical simulation of the mixing of two supersonic streams of air in a 25cm x 3cm flow field considering laminar velocity profile of the streams at inlet. They solved Euler equation and studied the effects of density, velocity and pressure variation on mixing. Brown and Roshko [3] experimentally investigated the effects of density ratio on plane turbulent mixing between two streams of different gases. It was observed that, for all ratios of densities in the two streams, the mixing layer was dominated by large coherent structures. These structures made convection at nearly constant speed, and increased their sizes and spaces discontinuously by the process of amalgamation with neighboring ones. Papamoschuo and Roshko [4] observed that the spreading rate was dependent on Mach number but independent on transverse density gradients. This was in good agreement with the experimental results of Debieve et al. [5] on different aspects of supersonic turbulent flows.

Ali et al. [6] studied the mixing mechanisms, investigated the mixing characteristics for several flow configurations and observed that recirculation in flow field can play an important role in the mixing enhancement. The authors found that the inlet configuration of air stream could play an important role on the enhancement of mixing. In an another investigation Ali et al. [7] studied the physics of mixing in two-dimensional supersonic stream and showed that mixing is only possible by the molecular diffusion terms in the Navier-Stokes equations. Gerlinger and Bruggemann [8] found that increase in injector lip thickness resulted in increased shear layer thickness and larger total pressure losses because of the stronger recompression shocks. They also found that increase in mixing layer thickness did not have significant effect on the mixing efficiency. Ali et al. [9] investigated the mixing layer for searching out the enhancement of mixing by varying the inlet width of air stream. It was found that the flow inlet configurations of mixing layers can play an important role on mixing. In another investigation Guirguis et al. [10] studied the effect of bluff center bodies on mixing enhancement in supersonic shear layers. They observed that the shear layer became unstable faster than with the streamlined body. As a result, a large amount of convective mixing occurs within the length of the domain. Azim and Islam [11] investigated plane mixing layers from parallel and non-parallel merging of two streams. The authors reported that both types of mixing layers were found to decrease in growth with increasing velocity ratio, though they spread more at the high speed side. Many other investigations also found that compressibility, characterized by the shear layer growth rate reduction has a vital effect on the supersonic mixing of the two streams.

In this present research, numerical investigation on supersonic mixing layers has been performed by solving two-dimensional unsteady Navier-Stokes equations, energy equation, mass diffusion equation and continuity equation. The problem is defined by allowing two streams past over a finite-thickness base (2.3 mm) confined between two parallel plates. The air stream of Mach 4.2 is at the upper side of the base plate and the hydrogen stream of Mach 1.1is underneath the base plate as shown in Fig. 1. After separating from the base, the streams form shear layers and mix with one another that usually occurs in combustor. This study has been made for the following reasons: (i) to increase the mixing efficiencies of a supersonic combustor and (ii) to study the physics of fluid dynamics including shocks and turbulence. The inlet pressure ratio and velocity ratio of the gaseous hydrogen to air streams have been kept constant at their values of 1.5 and 1.0 respectively. The merging angle is varied from 0 ~ 20º with the increment of 5º for this study. The calculations of flow field with different merging angles are denoted as case 1 (merging angle 0º), case 2 (merging angle 5º), case 3 (merging angle 10º), case 4 (merging angle 15º), and case 5 (merging angle 20º).

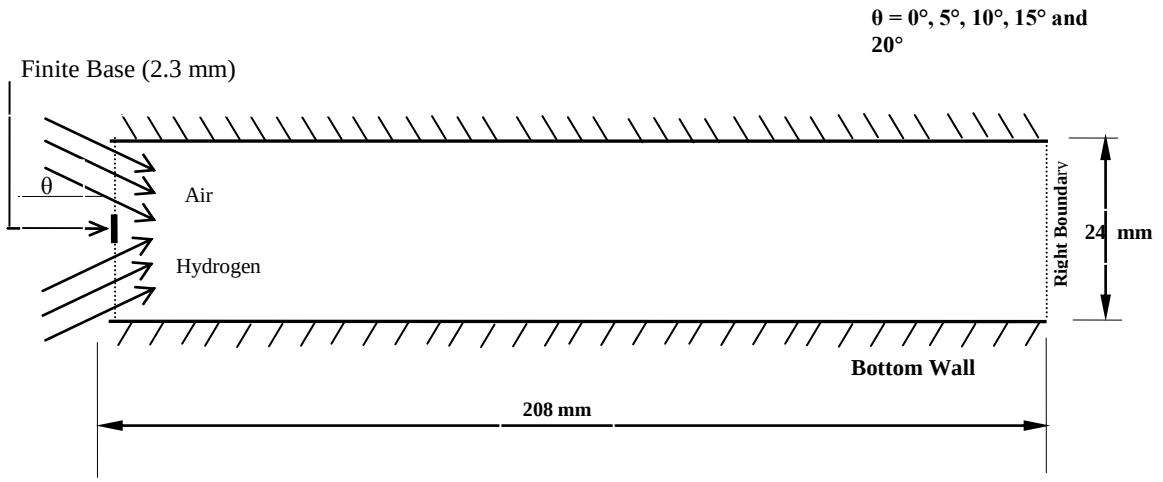

Fig. 1.Scematic diagram of the calculation domain

2. Governing equations and boundary conditions

The following continuity equation, Navier-Stokes equation, energy equation and mass diffusion equation are used to solve the flow field where body forces are neglected.

Continuity equation: $$\frac{\partial}{\partial t}(\rho)+\frac{\partial}{\partial x}(\rho u)+\frac{\partial}{\partial y}(\rho v)=0$$

Navier-Stokes equation: X component: $$\frac{\partial}{\partial t}(\rho u)+\frac{\partial}{\partial x}(p+\rho u^2)+\frac{\partial}{\partial y}(\rho uv)=\frac{\partial}{\partial x}(\sigma_x)+\frac{\partial}{\partial y}(\tau_{xy})$$

Y Component: $$\frac{\partial}{\partial t}(\rho v)+\frac{\partial}{\partial x}(\rho uv)+\frac{\partial}{\partial y}(p+\rho v^2)=\frac{\partial}{\partial x}(\tau_{yx})+\frac{\partial}{\partial y}(\sigma_y)$$

Energy equation: $$\frac{\partial}{\partial t}(E)+\frac{\partial}{\partial x}[(E+p)u]+\frac{\partial}{\partial y}[(E+p)v]=\frac{\partial}{\partial x}[u\sigma_x-v\tau_{xy}-\dot{q}_x]+\frac{\partial}{\partial y}[u\tau_{yx}-v\sigma_y-\dot{q}_y)]$$

Species continuity equation: $$\frac{\partial}{\partial t}(\rho Y_i)+\frac{\partial}{\partial x}(\rho Y_i u)+\frac{\partial}{\partial y}(\rho Y_i v)+\frac{\partial}{\partial x}(\dot{m}_{ix})+\frac{\partial}{\partial y}(\dot{m}_{iy})=0$$

- The top and bottom boundaries of the computational region are considered as solid walls. A Navier-Stokes analysis imposes that the normal and tangential velocity components are zero on the walls. The walls are assumed to be thermally adiabatic, so that $(\partial T/\partial n)_W=0$.
- Inflow boundary conditions are used on the left boundary of the computational domain. The inflow condition is supersonic with fully developed turbulent boundary layers which is kept constant throughout the computations. The outflow boundary conditions (X = L) are considered to be zero-gradient for all variables.

3. Results and Discussion

3.1 Physics of fluid dynamics

Figure 2 shows the velocity vectors with streamlines behind the finite base for case 1~5. In Fig 2(a~e) recirculation can be observed behind the thickness base. The stream lines indicate that the recirculation is created by the hydrogen flow. The portion of hydrogen in the recirculation makes intimate contact with air and deflects 180° due to the high momentum of air stream.

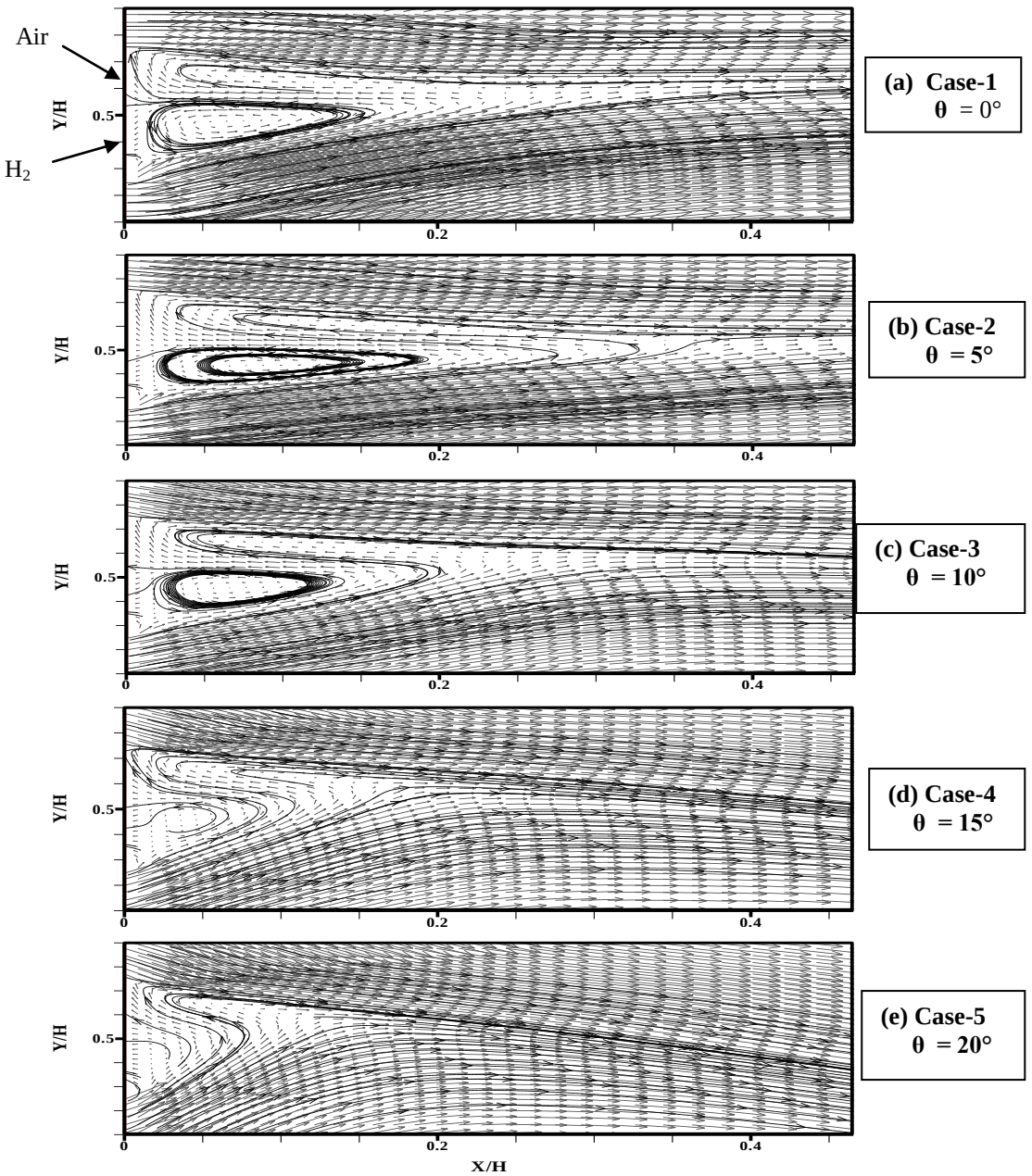

Fig 2. Vector and streamline representation of near flow circulating region for all cases.

Figure 2(a) shows that the shear layer mixing regions spread along the longitudinal distance from base until the impingement occurs approximately at X/H = 0.25, which is shorter than case 2. Therefore, the area of recirculation zone in case-1 is smaller than case-2. With the increment of merging angle the size of recirculation decreases, but the streamlines in Fig. 2(a~e) indicate that more hydrogen molecules enter into the upper side of the recirculation region and make intimate contact with the air stream. So strong interactions and eventually more molecular and convective diffusion of hydrogen occur at higher merging angles.

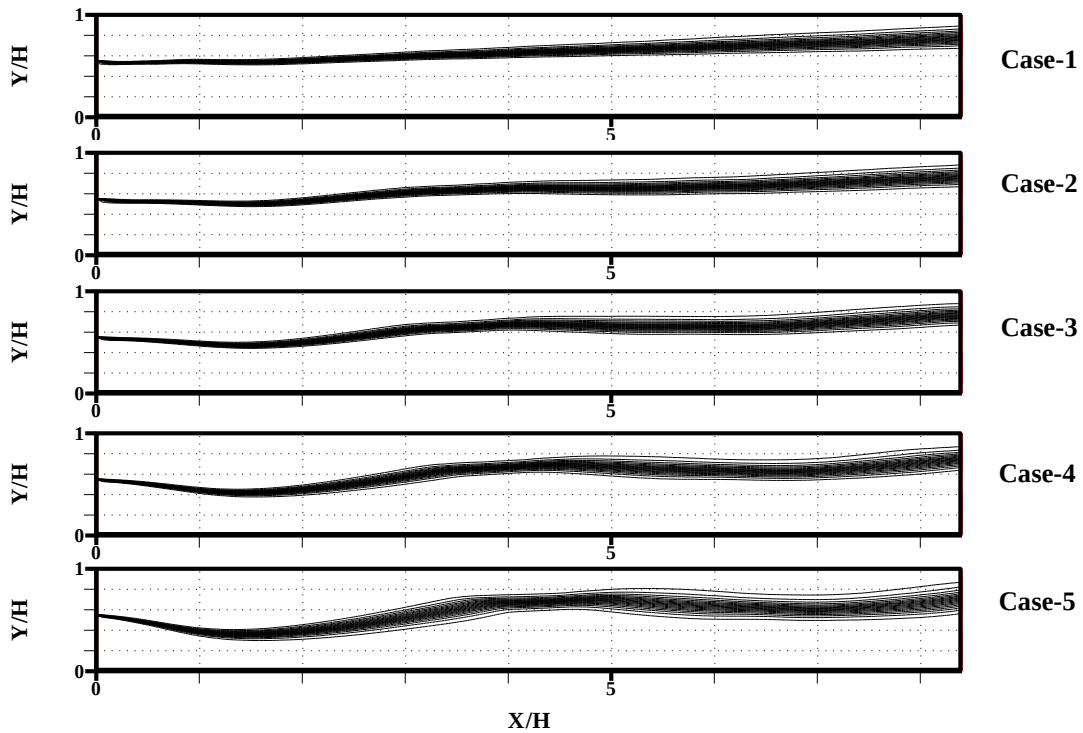

Fig. 3. Mole fraction contour of hydrogen φ (0.05, 0.95, 0.05) for different cases.

3.2 Structure of shear layers

The mole fraction contours give a structure of free shear layers created by the mixing of the two streams. Figure 3 shows the mole fraction contours of hydrogen for pressure ratio 1.5. The mole fraction of hydrogen close to bottom wall is 0.95 and the contour line varies from 0.95 to 0.05 towards the upper wall. The increment of mole fraction between two adjacent contour lines is 0.05. As stated earlier, a thin base is located from Y/H = 0.45 to 0.55 in the middle of the two streams. Since the hydrogen has less momentum than that of the air stream and merging angle is zero (Case-1) or low (Case-2), hydrogen occupies more space in the flow field. For high momentum the expansion of air is low in downstream. It can be pointed out that the inlet pressures of hydrogen and air are 1.5 atm and 1.0 atm, respectively. Due to higher pressure of hydrogen the shear layer deflects initially upward for case 1 (0^o merging angle). For cases 2~5 the shear layer deflects initially towards the bottom wall due to higher mass momentum of air. For all cases, spreading rate of hydrogen increases with the increase in merging angle. Closer to base thickness the deflection of air stream increases with the increase of merging angle and at far downstream all the shear layers deflect towards the upper boundary. The two hydrodynamic effects are found: firstly, the more expansion of

hydrogen for lower merging angle, and secondly, the wavy nature of shear layer for higher merging angles. Out of these two, higher merging angle causes strong interaction and dominates for increasing of mixing efficiency. In order to investigate in details, how the flow field structures are affected by the pressure ratios and merging angles, the computational domain should be long enough to allow the shear layer to become unstable.

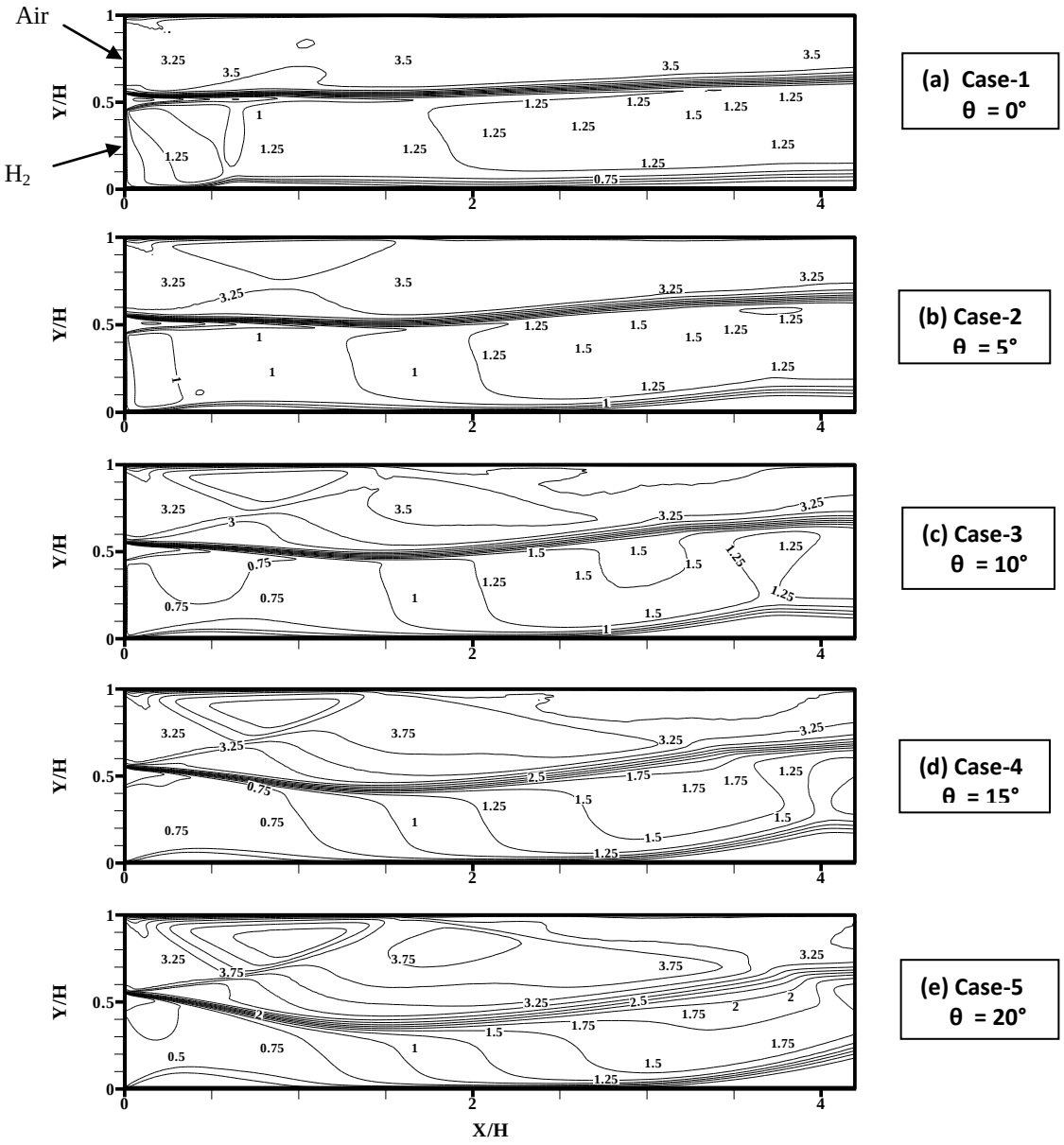

Fig. 4. Mach number contour for Case 1~5.

3.3 Mach number flow field

Mach number contours are also important for interpretation of the flow field characteristics and shown in Fig. 4 for cases 1~5. The free shear layers can be easily recognized by the dense contour lines in these figures. Due to higher momentum of air, the free shear layer follows straight line in case-1 without any disturbance by merging

angle. In other cases the wavy nature of shear layer can be found with downward deflection close to the base thickness. The first downward deflection of air stream creates obstacle to the hydrogen flow and consequently the Mach number of hydrogen decreases from supersonic to subsonic as found in Fig. 4(c~e). At far downstream the deflection of shear layer occurs towards upward direction, causes expansion of hydrogen stream and eventually the velocity increases to be supersonic. On the other hand, the upper flow of air is always supersonic and for case-1 the Mach number is approximately same all through the flow field. It is caused mainly due to the parallel stream of air and hydrogen (i.e. the merging angle is zero). However for the other cases the Mach number increases at far downstream due to the decrement of flow area and expansion of flow. Among cases 1~5, the Mach number of air is maximum at case 5 where the merging angle is the maximum. In this case the strongest interaction occurs causing higher mixing and the maximum expansion of flow at far downstream.

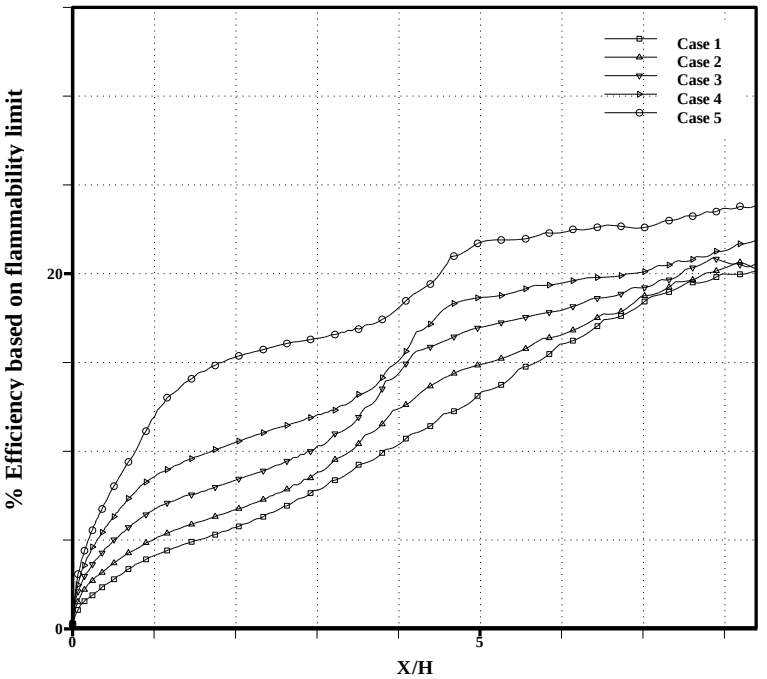

Fig. 5. Mixing efficiency based on flammability limit for different cases.

3.4 Mixing efficiency

Mixing efficiency has been calculated on the basis of flammability limits of hydrogen and air. So, in the calculation of mixing efficiency the region having the mole fraction ranges of hydrogen from 0.05 to 0.75 has been taken into consideration. The mixing of hydrogen in air can be occurred by means of (i) interaction between two streams, (ii) turbulence and convection due to recirculation and velocity of the flow, or (iii) molecular diffusion due to density gradient. The performance of different cases is evaluated by calculating the mixing efficiency. Figure 5 shows the mixing efficiency along the physical model for the different cases of the present numerical study. Generally, in the upstream region, the increasing of mixing is high and in downstream it is very slow. For all cases the mixing efficiency increases sharply just behind the base due to expansion behind the thin base and recirculation. The rate of increment in efficiency further occurs due to the interaction of two streams. In downstream the mixing is very slow in mixing shear-layer because weak molecular diffusion due to supersonic nature of the flow. Figure 5 shows that at X/H= 2 the mixing efficiencies of the cases 1, 2, 3, 4 and 5 are approximately 5.5, 6.5, 8.0, 10.0 and 20.5%, respectively, i.e., mixing efficiency increases with the increase of merging angle. The gradual increment of mixing can be found from case-1 to case-4 and suddenly high increment of mixing can be found from case-4 to case-5. With the wave of shear layer the considerable increment of mixing can be found in cases 2 to 5 at location of X/H

= 3.5 to 4.5. At far downstream, cases 3, 4 and 5 have small increment of mixing in the shear layer. Case 1 has almost constant increment of mixing along the length. In the flow field the maximum efficiency is about 28% and occurs in case-5 at outlet boundary.

4. Conclusion

Efficient mixing is the prerequisite for good combustion for a supersonic combustor. Many experiments, as well as theoretical and numerical studies have been conducted on mixing, ignition and combustion in supersonic flow. In supersonic combustion, high penetration and mixing of fuel with oxidizer is difficult due to their short residence time in combustor. In the present study the effects of merging angle (ranges from 0 ~ 20º) on supersonic mixing have been studied. Due to finite base, hydrogen and air expand behind the base creating a separation region and a recirculation region. Both hydrogen and air streams move to each other and strike behind base. The velocity in recirculation is low and therefore hydrogen has much time to contact with air resulting in high diffusion. By varying merging angle it has been found that, interaction between the two streams increases with increase of merging angle but the area of recirculation decreases. By the detail investigation of the recirculation region, it has been found that although recirculation area decreases with the increase of merging angle, high amount of hydrogen enters into the recirculation region and eventually mixing efficiency increases. Due to high interaction of the streams high momentum exchange occurs and eventually high mixing occurs at upstream for high merging angle. On the other hand, non-parallel mixing is least efficient in region and region and flow parameter investigated.

5. References

[1] Guirguis, R.H., Girnstein, F. F. Young, T. R. Oran, E. S. Kailashanath, K. and Boris, J. P., "Mixing Enhancement in Supersonic Shear Layers", 1987, AIAA 87-0373.

[2] Farouk, B., Oran, E. S. and Kailashanath, K., "Numerical Simulations of the structure of supersonic shear layers", Physics of Fluids, A, Vol. 3, No. 11 (1991), pp. 2786-2798.

[3] Brown, G.L., and Roshko, A., "On Density Effects and Large Structure in Turbulent Mixing Layers", Journal of Fluid Mechanics, Vol. 64, No. 4 (1974), pp. 775-816.

[4] Papamoschuo D., and Roshko, A., "The Compressible Turbulent Shear Layer: An Experimental Study", Journal of Fluid Mechanics, Vol. 197 (1988), pp. 453-477.

[5] Debieve, J., Dupont, P., Laurent, H., Menaa, M and Dussauge, J., "Compressibility And Structure Of Turbulence In Supersonic Shear Flows", *Eur. J. Mech.B-Fluids*, Vol. 19 (2000), pp. 597-614.

[6] Ali, M. Fujiwara, T. and Leblanc, J.E., "Influence of Main Flow inlet Configuration on Mixing and Flame Holding in Transverse Injection into Supersonic Air Stream", International Journal of Engineering Science, Vol. 38 (2000), pp.1161-1180.

[7] Ali, M. Fujiwara, T. and Parvez, A., "A Numerical Study on the Physics of Mixing in Two-dimensional Supersonic Stream", Indian Journal of Engineering and Materials Sciences, Vol. 9 (2002), pp.115-127.

[8] Gerlinger, P. and Bruggemann, D., "Numerical Investigation of Hydrogen Injections into Supersonic Airflows", Journal of Propulsion & Power, Vol. 16 (2000), pp.22-28.

[9] Ali, M. and Islam, A.K.M.S., 1999, "Effect of Main flow Inlet Width on Penetration and Mixing of Hydrogen in Scramjet Combustor", Proceedings o f the Eighth Asian Congress of Fluid Mechanics, pp. 647-650, December 6-10, Shenzhen, China.

[10] Guirguis, R.H. Girnstein, F. F. Young, T. R. Oran, E. S. Kailashanath, K. and Boris, J. P., "Mixing Enhancement in Supersonic Shear Layers: II. Effect of Bluff Centre Bodies", Laboratory for Computational Physics and Fluid Dynamics, Naval Research Laboratory, Washington, D.C., Report- 20375.

[11] Azim, M. A. and Islam, A.K.M.S., "Plane Mixing Layers from Parallel and Non-parallel Merging of Two Streams", Experiments in Fluids, Vol. 34 (2003), pp. 220-226.